NPS ARCHIVE
1961.09
HIGGINS, W.

Library
U. S. Naval Postgraduate School
Monterey, California

THERMAL BUCKLING OF CENTRALLY HEATED CIRCULAR DISCS WITH FIXED EDGES

A THESIS

SUBMITTED TO THE DEPARTMENT OF AERONAUTICAL ENGINEERING

AND THE COMMITTEE ON THE GRADUATE DIVISION

OF STANFORD UNIVERSITY

IN PARTIAL FULFILLMENT OF THE REQUIREMENTS

FOR THE DEGREE OF

ENGINEER

By

William Bernard Higgins

September 1951

NPS ARCHIVE
1961.09
HIGGINS, W.

Naval Postgraduate School
Monterey, California

ACKNOWLEDGMENT

The research described in this thesis was part of a general investigation conducted by the Department of Aeronautical Engineering at Stanford University and was sponsored by the United States Air Force Office of Scientific Research, Contract No. AF 49(638)-213.

The author is deeply grateful to Professor W. H. Horton for continuous and unstinting guidance and encouragement throughout the investigation and preparation of this paper. To Dr. N. J. Hoff and Nathyanarayana V. Hanagud for their timely assistance and suggestions, he is also grateful.

TABLE OF CONTENTS

		Page
ACKNOWLEDGMENT		iii
LIST OF ILLUSTRATIONS AND TABLES		v
NOTATION		vii
I.	INTRODUCTION	1
II.	TEST SPECIMENS AND APPARATUS	3
	2.1 Basic Experiment	3
	2.2 Test Specimens	3
	2.3 Plate Mounting and Heating	3
	2.4 Temperature Measurement	6
	2.5 Development of An Optical System for Buckling Determination	9
	2.6 Buckling Determination	10
III.	TESTING PROCEDURE AND RESULTS	15
	3.1 Scope of Testing	15
	3.2 Symmetry Checks	15
	3.3 Accumulation of Data and Experimental Results	15
	3.4 Extension of Experimental Investigation	15
IV.	THEORY	21
	4.1 Assumptions	21
	4.2 Equations of Plane Thermal Stress	21
	4.3 Equations of Buckling	23
V.	ANALYSIS AND CONCLUSIONS	25
	5.1 Comparison of Experimental Results with Theoretical Critical Temperatures	29
	5.2 The Buckling Parameter, τ_0	31
	5.3 Conclusions	32
APPENDIX I.	An Optical Method for the Determination of Buckling Deflections	35
APPENDIX II.	Calculation of Theoretical Critical Temperature Using the Vianello-Stodola Method and Experimental Data	50
APPENDIX III.	Sample Calculations	54
REFERENCES		64

LIST OF ILLUSTRATIONS

Figure		Page
1	Typical Test Plates	4
2	Mounting Rings	5
3	Test Stand	7
4	Thermocouple Location	8
5	Typical Oscillograph Record	10
6	Rejected Plate Fringe Pattern	11
7	Experimental Equipment	13
8	Unbuckled Plate Fringe Pattern	14
9	Buckled Plate Fringe Pattern	14
10	Thermocouple Location for Temperature Symmetry Check	16
11	Temperature Distribution Curves	18
12	Buckling Stress Distribution	19
13	Buckling Parameter-Temperature Distribution Plot	33
14	Temperature Distribution Curves	34

APPENDIX I:

1	Fringe Phenomenon	38
2	Fringe Phenomenon	38
3	Fringe Phenomenon	38
4	Light Ray Reflection	40
5	First Stage Apparatus	42
6	First Stage Fringe Pattern	42

LIST OF ILLUSTRATIONS (Continued)

Figure		Page
7	Geometry of Optical System	44
8	Proposed System	45
9	Fringe Pattern Before Buckling	48
10	Fringe Pattern After Buckling	48

APPENDIX II:

II-1	Experimental and Approximated Temperature Distribution	52
II-2	Experimental and Approximated Temperature Distribution	57

APPENDIX III:

III-1	Temperature Distribution, Run No. 50512	62
III-2	Tr vs. r Plot	63

LIST OF TABLES

I	Data and Results	37
II	Temperature Reduction, Run 50512	60

NOTATION

r, ω	Polar coordinates
T	Temperature rise above ambient
T_c	Temperature rise above ambient at $r = 0$
θ	Non-dimensionalised temperature, T/T_c
σ_r, σ_ω	Radial and tangential normal stresses
ρ	r/b
b	Outer radius of disc
t	Thickness of disc
ϵ_r, ϵ_ω	Unit elongation in radial and tangential directions
ν	Poisson's ratio
u, v, w	Displacements in the r, ω, z directions
α	Coefficient of thermal expansion
E	Modulus of elasticity
F	Stress function
N_x, N_y, N_{xy}	Forces per unit length
$D = Et^3/12(1-\nu^2)$	Flexural rigidity of plate
ϕ	dw/dr

NOTATION (Continued)

$\tau_o = \frac{12(1-\nu^2)R^2}{t^2}\tau_n$ Scaling parameter

$\sigma = -\frac{\sigma_x}{\gamma H \tau_o}$ Stress parameter

1. INTRODUCTION

Thermal stress theory, like so many other theoretical theories of the physical sciences, was well established before the present technological era. Duhamel, as early as 1837, included in his study of elastic theory the effects of temperature variation.[1] Structural application of such theory was made in the development of steam engines, steam turbines, and locomotives. However, the recent development of nuclear power, space vehicles, supersonic aircraft and similar devices, where large amounts of power are expended in small space, has intensified the demand for further research and study of this aspect of material behavior.

Thermal stress, produced by temperature gradients resulting from transmission of heat flow, can cause structural collapse either from material failure or by causing instability (buckling). Buckling may be considered in two categories. One of these is of a time-dependent nature (creep). This phase has been extensively investigated by Boley.[2] The other category, in which this investigation lies, is that in which the buckling is due solely to thermal gradients.

Buckling, whether due to normal loading or to thermal gradients, is a prime consideration in the design of high-speed aircraft, rocket motor components and structural aspects. In particular, wing and fuselage design must include consideration of the thermal stresses arising from supersonic flight, burning of hot propellant gases, and intense aerodynamic and solar heating.

For references, see page 23.

This investigation attempts to relate experimental observations to theoretical predictions of the buckling behavior of circular plates loaded solely by centrally applied hot spots. The case considered is that of the fixed-edge condition. This problem is to a considerable degree analogous to the plane stress elastic problem of the thin disc compressed by a uniformly distributed edge loading.[5]

II. TEST SPECIMENS AND APPARATUS

2.1 Basic Experiment

Local heating in the plane of a thin disc results in a thermal stress distribution, which at a certain critical level will cause buckling out of the plane. When centrally applied, the stress distribution is axisymmetric, and a solution of the thermoelastic stability equations becomes attainable. The purpose of this investigation was to perform experimental tests to obtain data on buckling behavior of the test plates and to obtain a theoretical solution against which these data might be compared.

2.2 Test Specimens

To achieve a stress distribution approximately that of plane stress, one must compromise between a plate thickness such that a temperature gradient (and therefore a stress gradient) exists across the thickness, and one so thin that initial flatness is no longer a reasonable assumption. Three considerations governed the choice of test plate thickness.

Two test discs were used. Disc No. 1 was 1020 cold-rolled steel, 0.074 in. in thickness and 12 in. in diameter. Disc No. 2 was 2024 or 4355 aluminum, 0.064 in. in thickness and 12 in. in diameter. Use of optical equipment described in Section 2.5 permitted the selection of test discs which were to a high degree initially flat and free of surface imperfections. Typical test plates are shown in Fig. 1.

2.3 Plate Mounting and Heating

The test discs were fixed in steel mounting rings, shown in Fig. 2. These rings were one inch thick, of outer diameters 17 in. and 12 in., and provided the dual requirement of edge fixity and heat sink. This mounting arrangement resulted in a 10.0 in. span of the test plates.

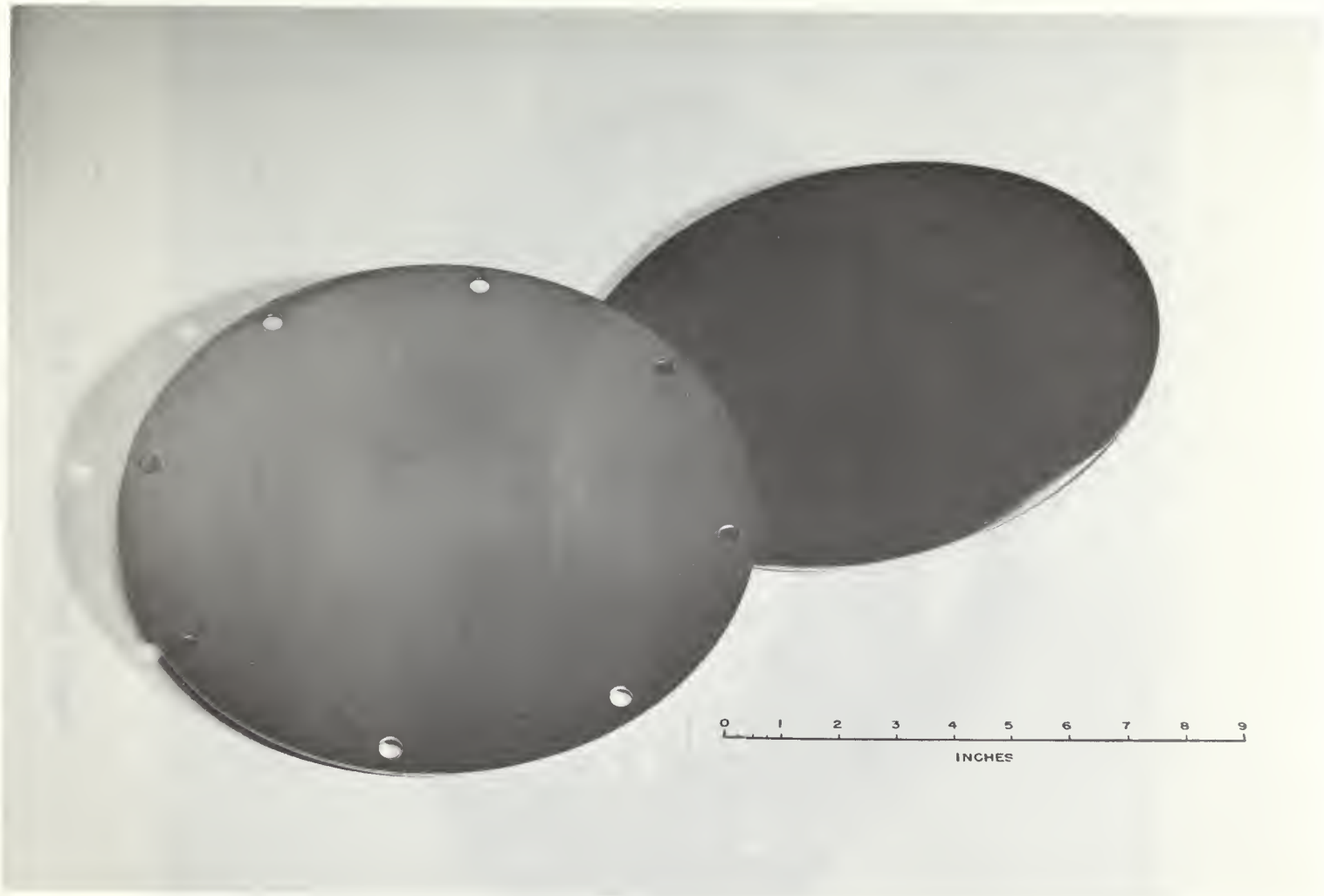

Fig. 1 Typical Test Plates

The mounting ring-test disc combination was supported by a steel test stand to which auxiliary equipment was attached. Source of heat was a Westinghouse 300R/3FL special service lamp, 220 volts supply, mounted below the test plate. Varying temperature distributions were obtained by changing the diameter of the hot spots through use of annular reflectors of sandwich construction, placed on similar mounting reflectors on the underside of the test stand. These reflectors consisted of double thicknesses of reflective aluminum separated by 3/16 in. spacers. In addition, a one-inch layer of glass wool between the reflectors and the test plate served to localize the application of heat energy. Layers of woven glass fiber were used to diffuse the lamp radiation to achieve an axisymmetric temperature distribution.

The test stand, mounting rings, lamp and reflectors are shown in Fig. 3.

2.4 Temperature Measurement

Temperatures were measured by chromel-alumel thermocouples. Fusing of the chromel and alumel wires into the thermocouple bead and the attachment of the thermocouple to the plate were done by using a portable capacitor-discharge welder designed and built in the laboratory. This device has variable capacity and discharge rate features, which allow the thermocouples to be attached to materials of varying physical properties.

Eleven thermocouples were placed on the five-inch radius of the test plate, spaced at one-quarter and one-half inch intervals where the gradient was steep, and at greater spacing elsewhere. Spacing varied slightly for the steel and aluminum plates, depending on what was required to obtain a proper distribution. Thermocouple location for the aluminum plate is shown in Fig. 4.

The thermocouple voltages were recorded on a Consolidated Engineering Corporation Oscillograph, Type 5-101B, with a room temperature reference junction. The oscillograph galvanometers were calibrated with a Leeds and Northrup portable potentiometer. Typical galvanometer

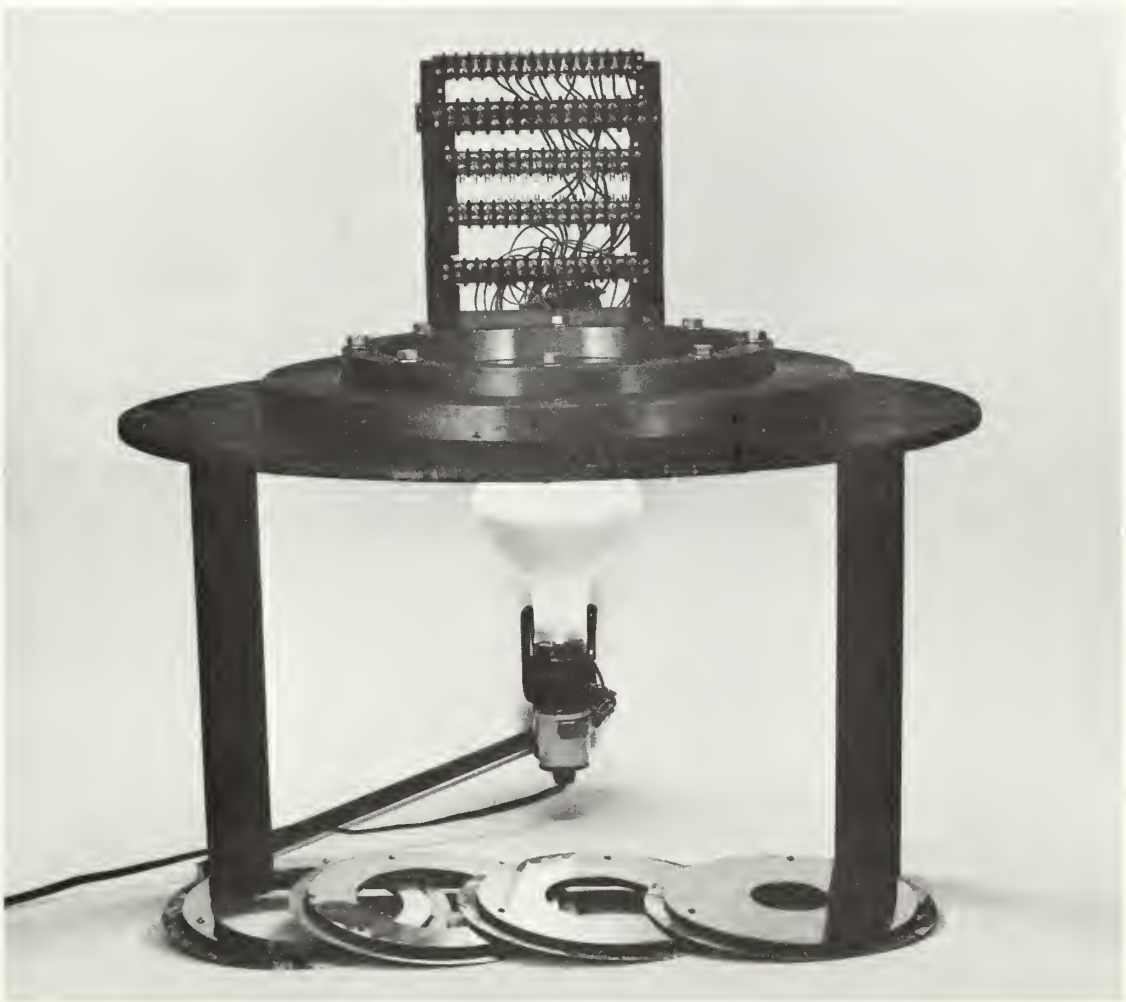

Fig. 3 Test Stand

TC No.	Distance from Center
1	0
2	0.45 in.
3	0.73
4	0.98
5	1.24
6	1.52
7	1.96
8	2.50
9	3.00
10	3.50
11	4.00

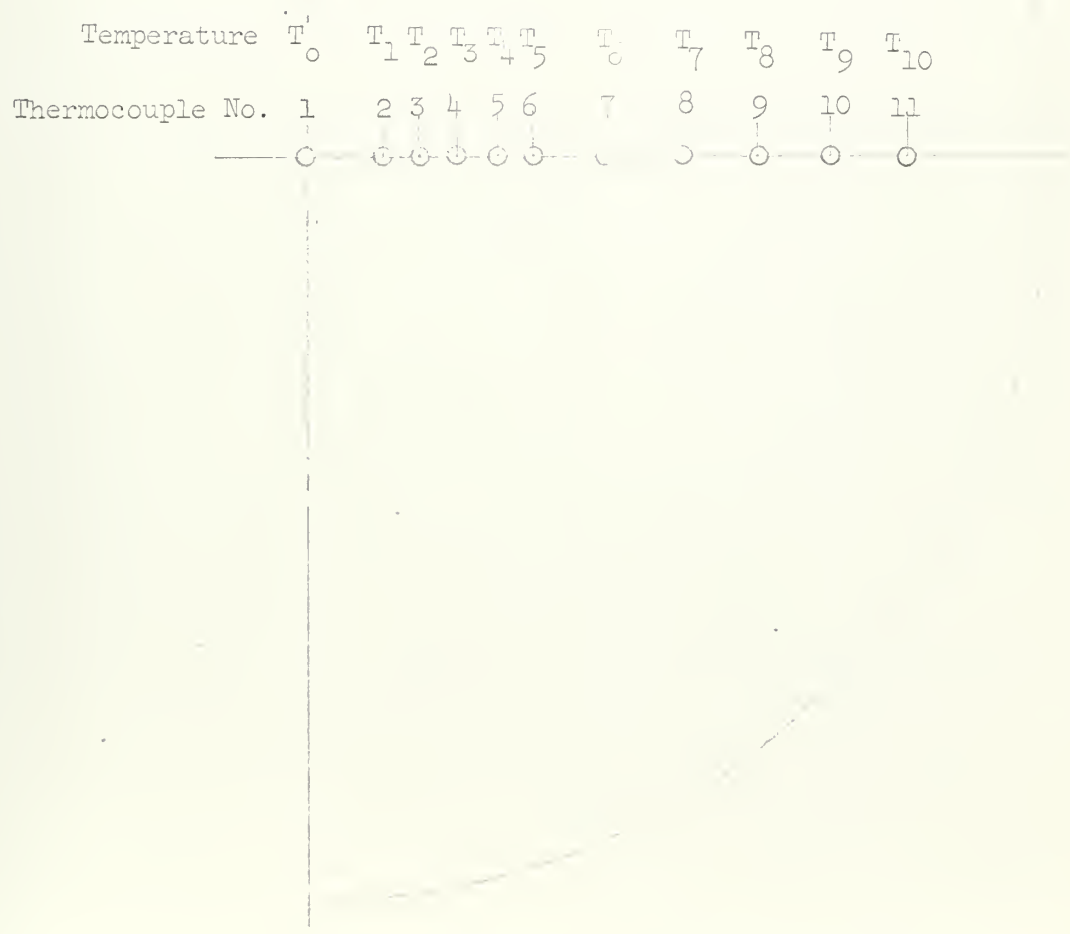

Fig. 4 Thermocouple Location
(Aluminum Plate)

sensitivity was on the order of two inches of galvanometer swing per millivolt. A Coleman Oscillograph Reader was used in the evaluation of the oscillograph tape. The reader had a scale of 300 reader units per inch of galvanometer swing. Accuracy in using the reader is estimated at 3 units, corresponding to 0.005 millivolts, or about one-quarter degree fahrenheit. A typical oscillograph record is shown in Fig. 5.

Preliminary tests showed substantial temperature fluctuations due to convection currents about the thermocouples. Covering them with fire clay powder solved this problem and reduced possible radiation losses.

2.5 Development of an Optical System for Buckling Determination

Proper experimental technique in determination of buckling of thin plates not only requires the time-oriented detection of very small displacements, but also that the buckling is not influenced by the method of observation. Any loading normal to the surface of the plate, such as that created by a dial gage, will have an obvious effect on the test results.

In the early stages of this experimental work, considerable study was given to a number of transducers, including variable reluctance, linear potentiometer, and capacity types. In each case, the same conclusion was reached: there was to some degree an undesirable interaction. Some type of optical system seemed feasible, and after research an application of the Moire mechanical interference fringe principle was selected. With this technique the specimen, or a segment of it, becomes part of a mirror system. Basically, displacement of a projected parallel line system occurs when the slope of the plate changes. This displacement, in effect highly magnified by use of another system of slightly skewed lines, is projected on a milk glass plate for observation and photographing. The Moire method is described in Appendix I.

Development of the optical system produced some unexpected advantages. The high sensitivity of the system allowed an excellent inspection for initial flatness and surface defects. Fig. 6 shows the fringe pattern for a plate rejected because of two dimples approximately 0.002 in. in depth. Deflections of 0.0005 to 0.0010 in. were consistently detectable by eye.

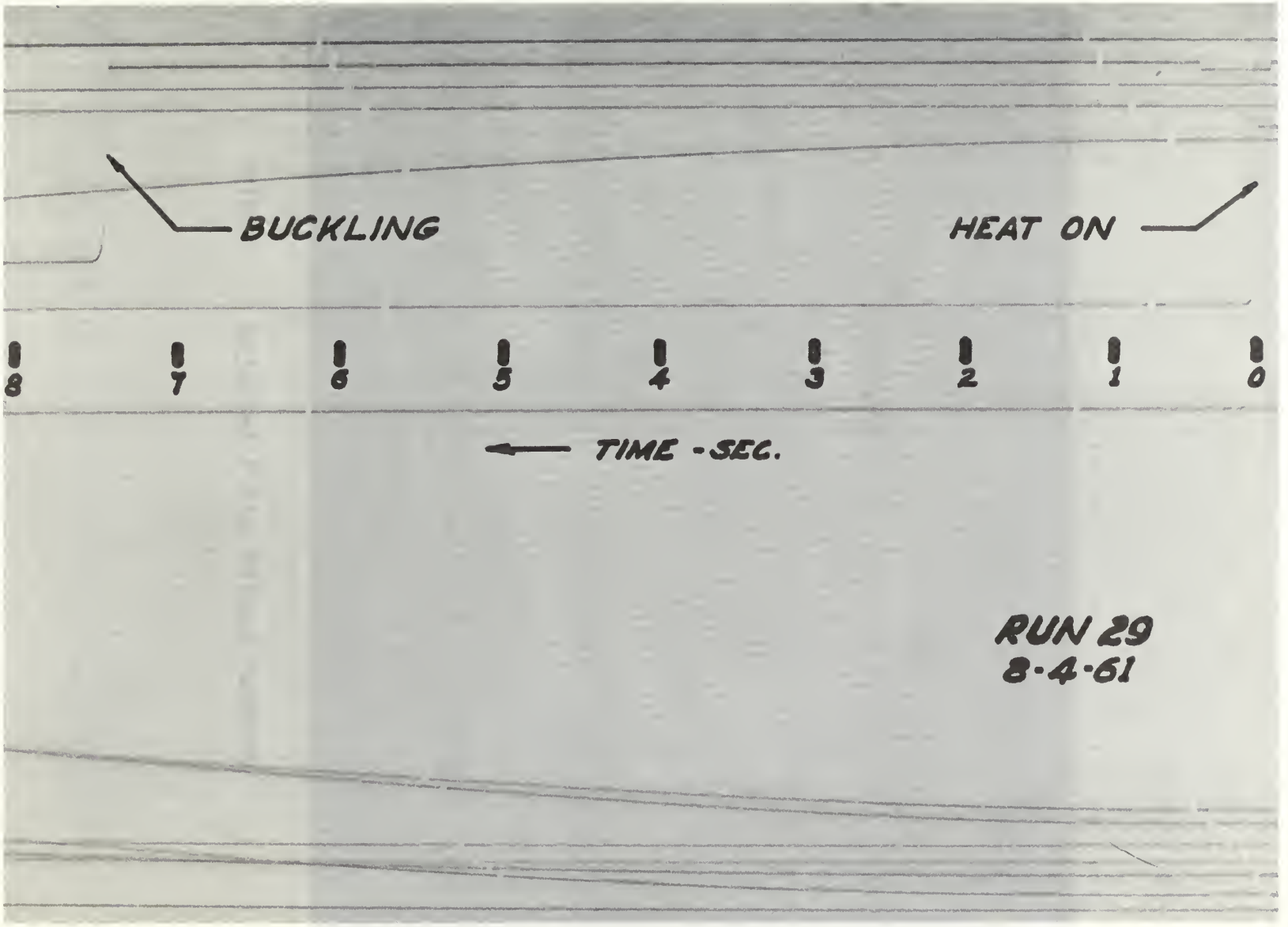

Fig. 5 TYPICAL OSCILLOGRAPH RECORD

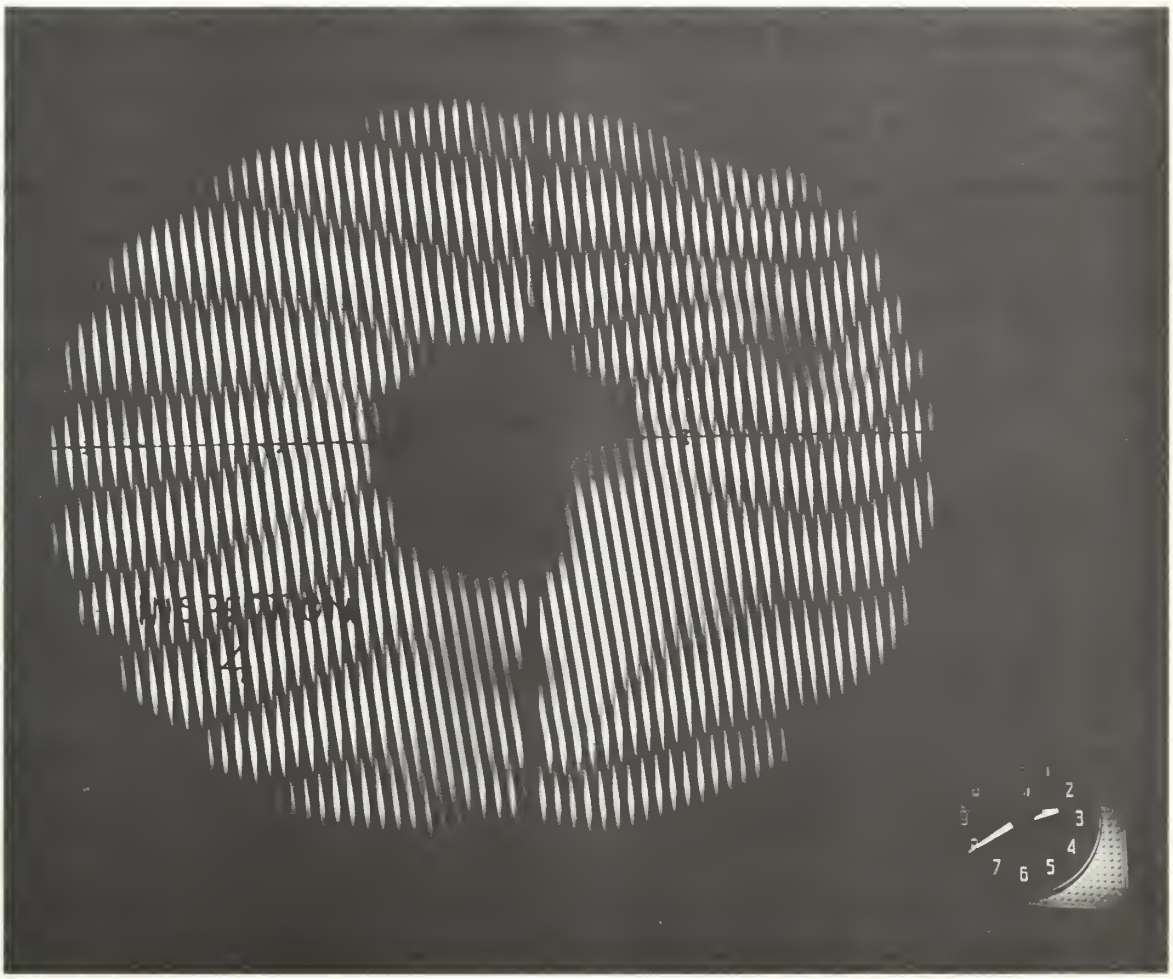

Fig. 6 Rejected Plate Fringe Pattern

3.0 Buckling Determination

Experimental equipment is shown in Fig. 7. A fringe pattern is faintly discernible on the milk glass viewing plate. On the camera side of the glass, initial position of the fringe was indicated by a chinn-marking pencil. An electric clock with sweep second hand was mounted in the camera field. A Bell and Howell motion picture camera, with Eastman Tri-X reversal film underexposed for contrast, was used to record fringe movement. In addition to the film record, a manual input of voltage to one of the oscillograph channels at buckling onset and a stopwatch, gave additional checks on buckling time.

Fringe patterns before and after buckling are shown in Figs. 8 and 9 respectively.

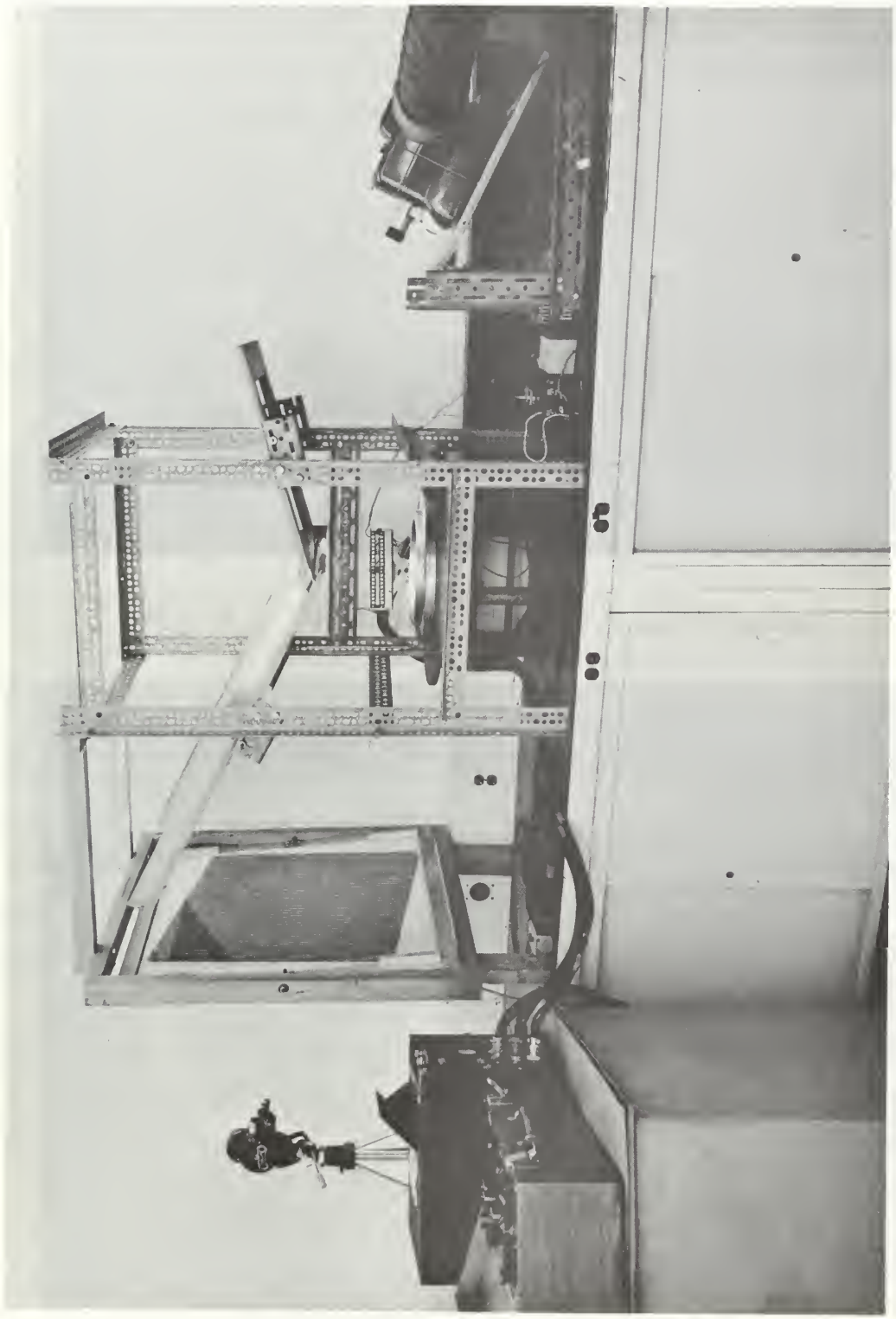

Fig. 7 Experimental Equipment

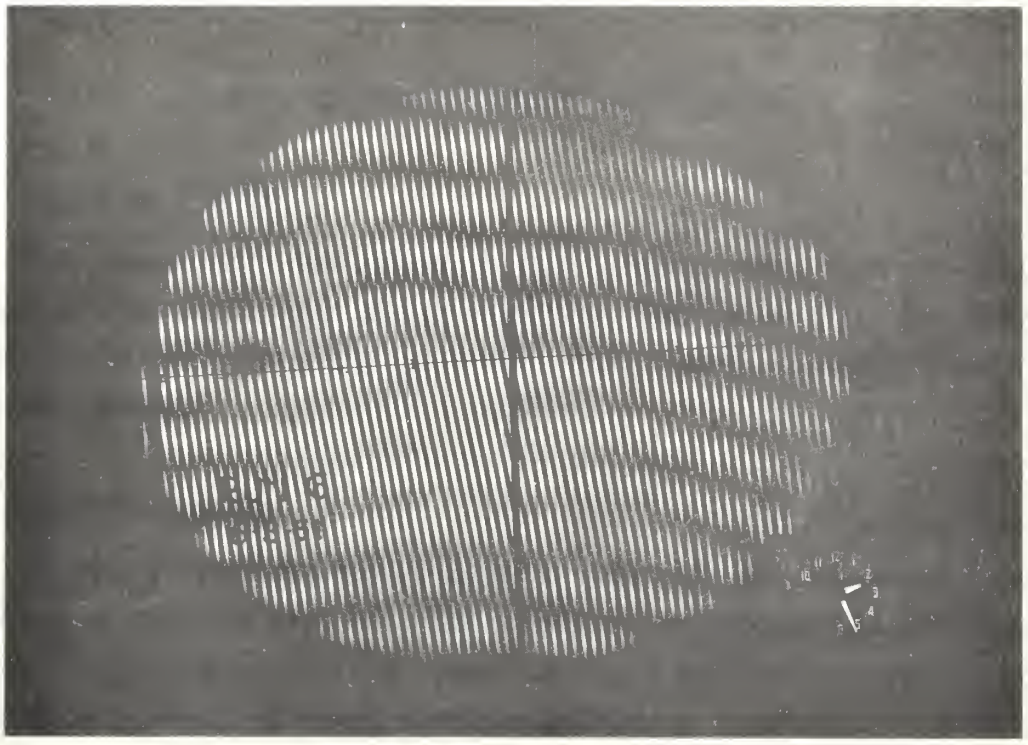

Fig. 8 Unbuckled Plate Fringe Pattern

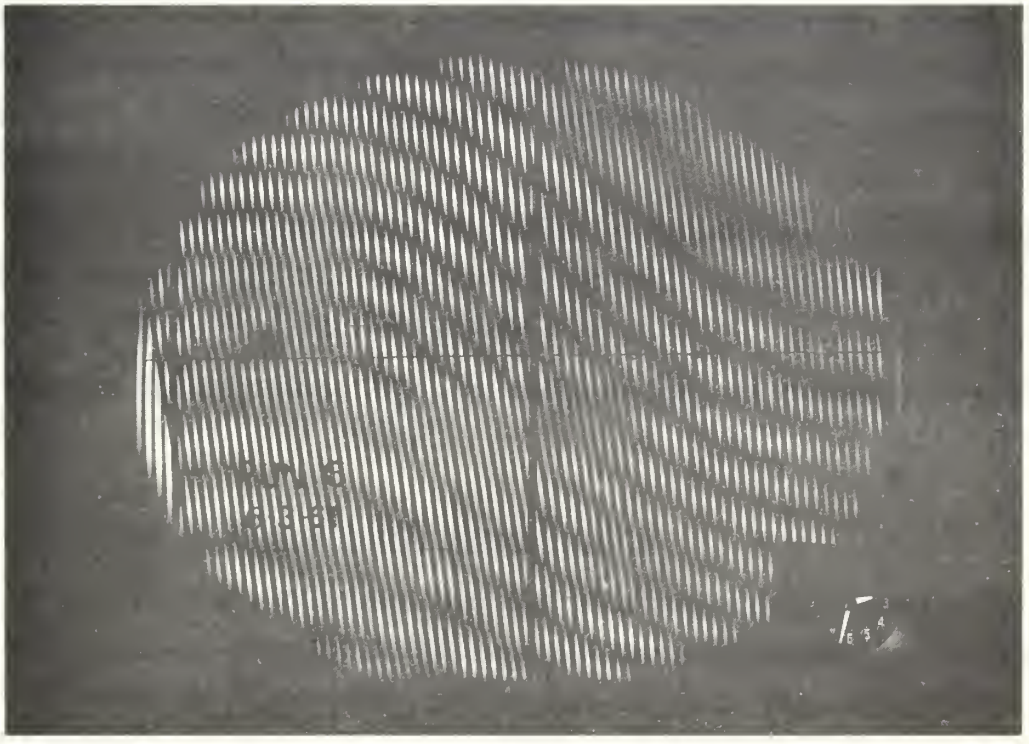

Fig. 9 Buckled Plate Fringe Pattern

III. TESTING PROCEDURE AND RESULTS

3.1 Scope of Testing

Two temperature distributions for each test disc were obtained by using annular reflectors having variable sized holes (Fig. 3). For steel, two- and three-inch holes were used, and for aluminum, one- and two-inch holes.

3.2 Symmetry Checks

To check symmetry, test runs were made with the thermocouple configuration shown in Fig. 10. The variation in temperatures for thermocouples equidistant from the center averaged one-quarter degree, the estimated accuracy of temperature measurement.

3.3 Accumulation of Data and Experimental Results

In addition to the symmetry checks, preliminary runs were made to achieve consistent results. Inconsistencies such as those caused by convective currents were eliminated before recording data from eight runs, shown in Table I. Sample calculations for Run No. 5/5lt are given in Appendix III.

A plot of the temperature distribution parameter, θ, for typical runs is shown in Fig. 11. The curves are well approximated by a second-degree curve (Fig. II-1, page 52).

Stress distribution, σ_r, is shown in Fig. 12 for four of the test runs.

3.4 Extension of Experimental Investigation

Temperature distribution data can be considerably augmented by use of larger plates, varying thicknesses and materials; and the results compared with the theoretical predictions based on Fig. 13 and Fig. 14 (Section 5.2).

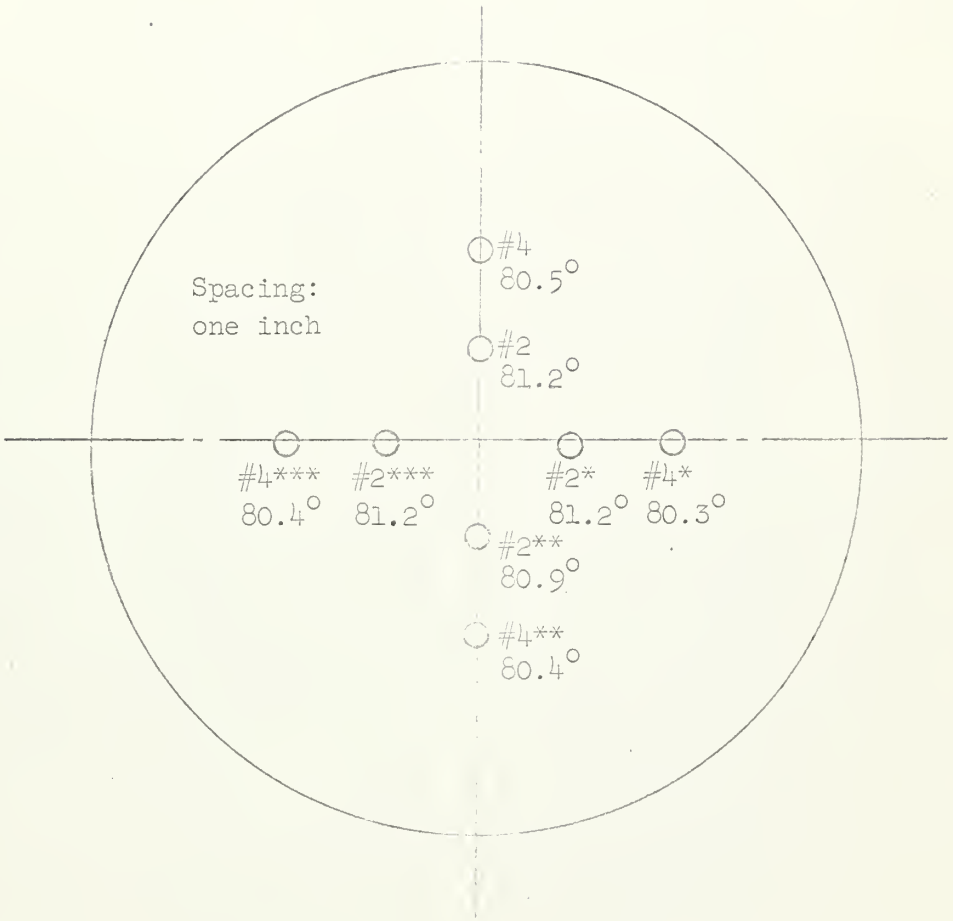

Fig. 10 Thermocouple Location for Temperature Symmetry Check

TABLE I

DATA AND RESULTS

RUN IDENTIFIER	MATERIAL	HOT SPOT DIAMETER	Temperature at Buckling, ^{o}F											$\sigma_{r_{max}}$ (psi)	Buckling Time (seconds)
			T_o	T_1	T_2	T_3	T_4	T_5	T_6	T_7	T_8	T_9	T_{10}		
59493	Steel	2 in.	94.4	*	102.0	90.0	72.4	54.8	35.9	32.0	21.5	17.3	6.9	-	107
[illegible]	[illegible]	2 in.	93.2	90.7	80.3	70.0	68.0	51.0	31.7	28.7	17.5	14.5	4.0	-13,000	[illegible]
59590	Steel	3 in.	120.0	78.1	73.0	56.6	38.5	26.8	14.7	7.5	4.0	2.8	0	-10,600	33
[illegible]	Steel	3 in.	118.0	81.0	65.0	50.4	33.5	24.0	12.2	6.2	2.7	1.5	0	-	33
59665	Aluminum	1 in.	19.7	17.2	14.8	13.5	11.0	9.7	7.5	4.2	3.3	2.2	1.4	- 1,810	61
59669	Aluminum	1 in.	20.2	18.5	14.9	14.8	11.9	10.3	6.3	5.2	3.2	2.4	1.4	-	68
59675	Aluminum	2 in.	26.8	23.5	19.7	21.0	15.4	14.1	6.5	5.4	3.1	2.3	1.5	- 2,450	24
59702	Aluminum	2 in.	26.4	20.2	21.0	19.0	17.0	12.7	8.7	7.2	4.5	3.0	1.6	-	22

* trace faded out

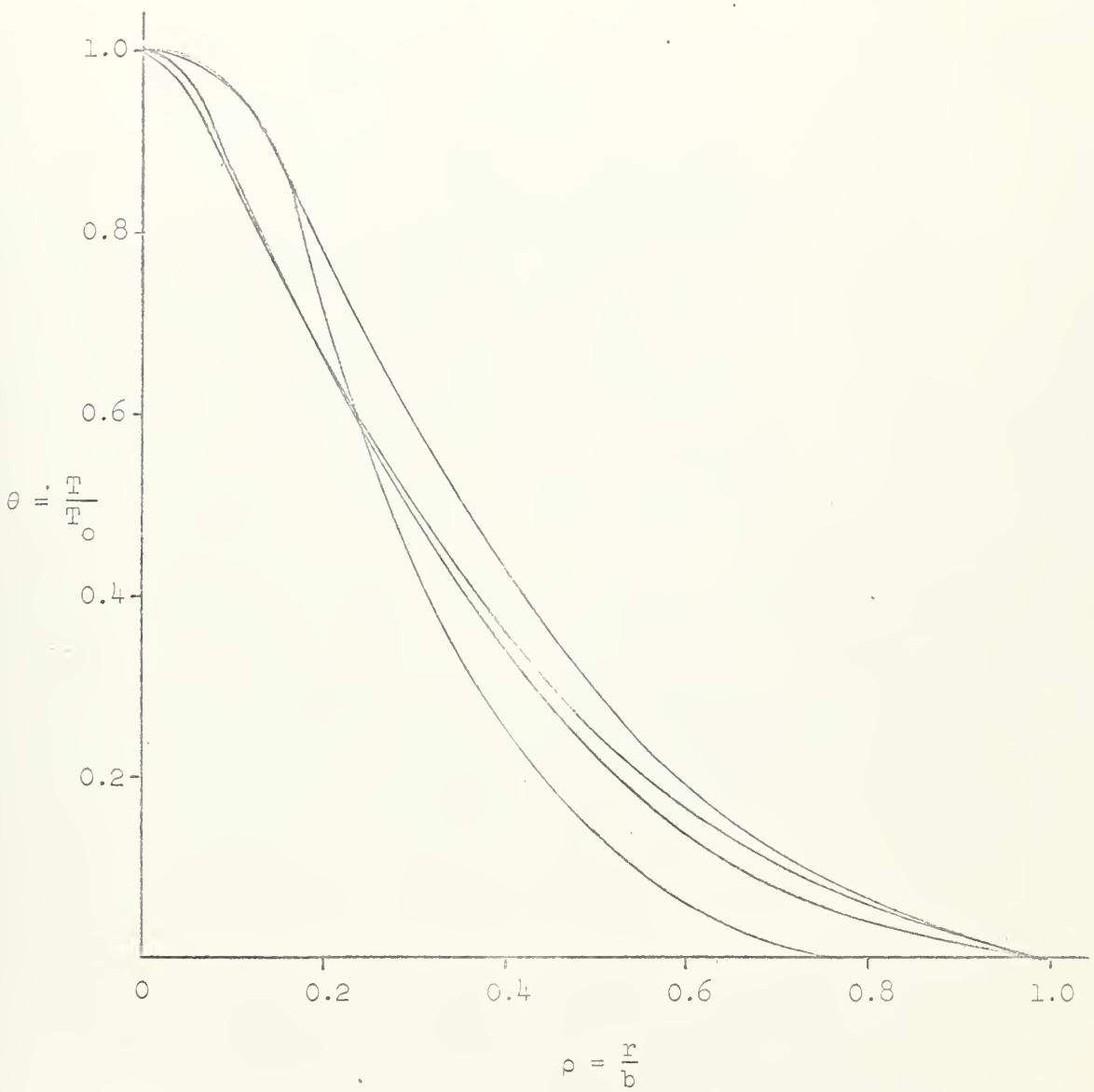

Fig. 11 Temperature Distribution Curves

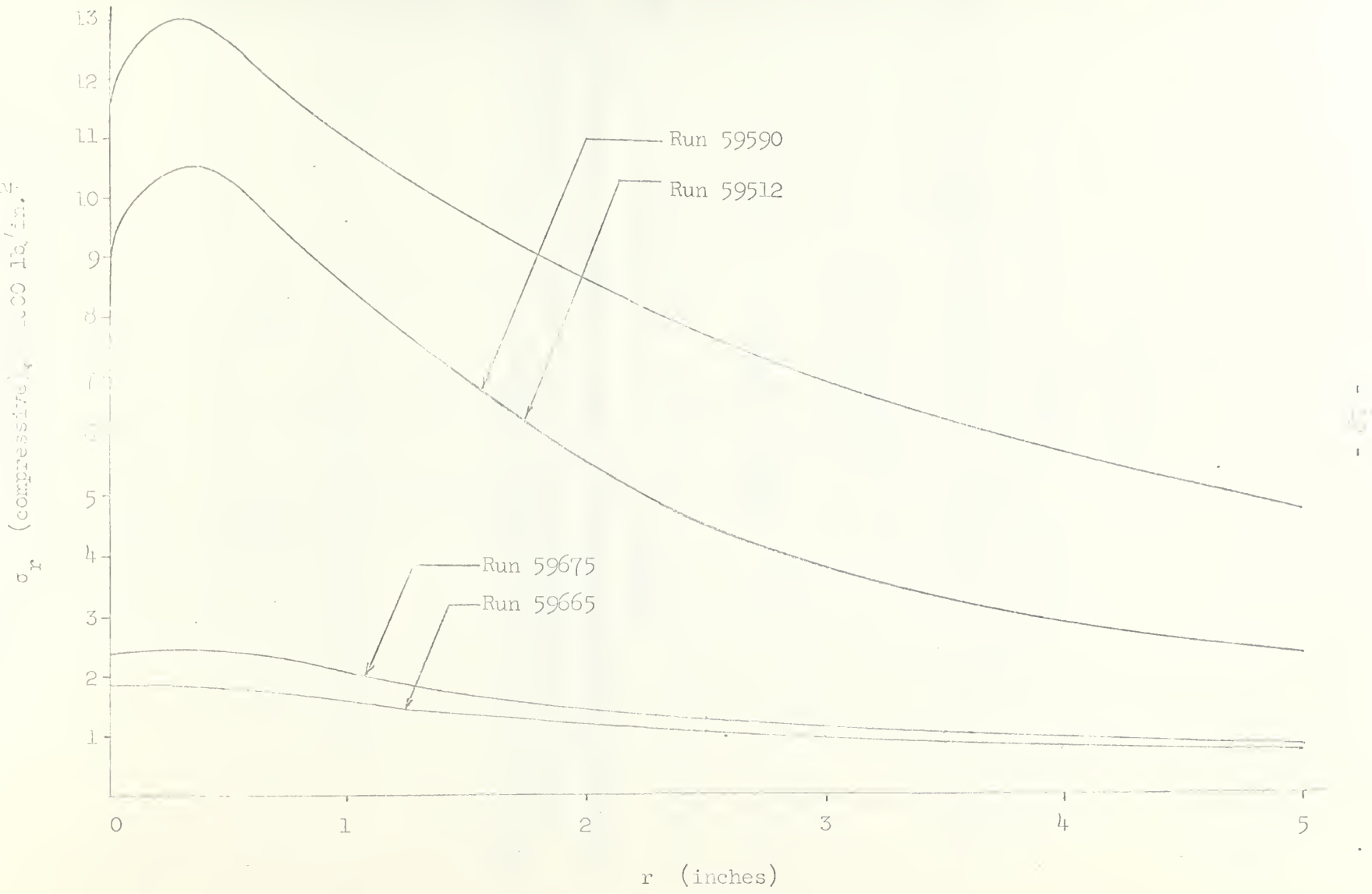

Fig. 12 Buckling Stress Distribution

With additional data, it should be possible to establish the relationship between the heat energy input, Q, and the critical central temperature, T_c, and the buckling time, τ:

$$T_c = AQ^n$$

$$\tau = BQ^m$$

where A, B, n, and m would be determined from experimental results, and from the relation:

$$Q = \int_V \rho c T \, dV$$

$$= 2\pi\rho ct \int_0^b Tr\,dr$$

where c is the specific heat and ρ is the density.

An interesting extension in this field of investigation might be to perform tests with non-concentric hot spots to determine the buckling behavior and to derive a space parameter related to the non-concentricity.

IV. [illegible]

4.1 Assumptions

The following basic assumptions are made in the theoretical development:

1. Temperature distribution and edge restraint are axisymmetric.
2. The plate is flat, uniform in thickness, initially unstressed and at uniform temperature.
3. The material is perfectly elastic, homogeneous and isotropic.

4.2 Equations of Plane Thermal Stress

For the assumptions of Section 4.1, the equation of equilibrium can be written as:[4]

$$\frac{d\sigma_r}{dr} + \frac{\sigma_r - \sigma_\omega}{r} = 0 \qquad (4.2.1)$$

The stress-strain relations for plane stress, modified for thermal expansion, are:

$$\epsilon_r - \alpha T = \frac{1}{E}(\sigma_r - \nu\sigma_\omega)$$
$$\epsilon_\omega - \alpha T = \frac{1}{E}(\sigma_\omega - \nu\sigma_r) \qquad (4.2.2)$$

The strains in terms of the radial displacement, u, are:

$$\epsilon_r = \frac{du}{dr}, \qquad \epsilon_\omega = \frac{u}{r} \qquad (4.2.3)$$

Solving (4.2.1) for the stresses:

$$\sigma_r = \frac{E}{1-\nu^2}\epsilon_r + \nu\epsilon_\omega - (1+\nu)\alpha T$$
$$\sigma_\omega = \frac{E}{1-\nu^2}\epsilon_\omega + \nu\epsilon_r - (1+\nu)\alpha T \qquad (4.2.4)$$

Combining (4.2.1) and (4.2.4):

$$r\frac{d}{dr}(\sigma_r + \nu\sigma_\theta) + (1-\nu)(\sigma_r - \sigma_\theta) = (1+\nu)\alpha r\frac{dT}{dr} \tag{4.2.5}$$

Equation (4.2.5) in terms of the displacement relation (4.2.3) becomes:

$$\frac{d^2u}{dr^2} + \frac{1}{r}\frac{du}{dr} - \frac{u}{r^2} = (1+\nu)\alpha\frac{dT}{dr} \tag{4.2.6}$$

Integration of (4.2.6) gives the displacement:

$$u = (1+\nu)\alpha\frac{1}{r}\int_0^r Tr\,dr + C_1 r + \frac{C_2}{r} \tag{4.2.7}$$

Combining (4.2.7) with (4.2.3) and (4.2.4) one obtains the stress relations:

$$\sigma_r = -\frac{C_2}{r^2}\int_0^r Tr\,dr + \frac{E}{1-\nu^2}\left\{C_1(1+\nu) - C_2\frac{(1-\nu)}{r^2}\right\} \tag{4.2.8}$$

and

$$\sigma_\theta = \frac{C_2}{r^2}\int_0^r Tr\,dr - \alpha ET + \frac{E}{1-\nu^2}\left\{C_1(1+\nu) + C_2\frac{(1-\nu)}{r^2}\right\} \tag{4.2.9}$$

The boundary conditions for the fixed-edge case are:

$$\begin{aligned} u(0) &\text{ is finite} \\ u(1) &= 0 \end{aligned} \tag{4.2.10}$$

The first boundary condition, applied to (4.2.7) gives $C_2 = 0$, since:

$$\lim_{r \to 0} \frac{1}{r} \int_0^r Trdr = 0$$

Applying the second boundary condition, one obtains:

$$C_1 = -\frac{(1+\nu)}{b^2} a \int_0^b Trdr$$

The fixed-edge stresses are then given by:

$$\sigma_r = -\frac{a}{r^2}\left\{\int_0^r Trdr + \frac{r^2(1+\nu)}{b^2(1-\nu)}\int_0^b Trdr\right\} \qquad (4.2.11)$$

$$\sigma_\theta = \frac{a}{r^2}\left\{\int_0^r Trdr - Tr^2 - \frac{r^2(1+\nu)}{b^2(1-\nu)}\int_0^b Trdr\right\} \qquad (4.2.12)$$

4.3 Equations of buckling

The general equations for bending of thin plates are:[5]

$$\nabla^4 F = \frac{\partial^4 F}{\partial x^4} + 2\frac{\partial^4 F}{\partial x^2 \partial y^2} + \frac{\partial^4 F}{\partial y^4} = E\left\{\left(\frac{\partial^2 w}{\partial x\, \partial y}\right)^2 - \frac{\partial^2 w}{\partial x^2}\frac{\partial^2 w}{\partial y^2}\right\} \qquad (4.3.1)$$

$$\nabla^4 w = \frac{1}{D}\left\{q + \frac{\partial^2 F}{\partial y^2}\frac{\partial^2 w}{\partial x^2} + \frac{\partial^2 F}{\partial x^2}\frac{\partial^2 w}{\partial y^2} - 2\frac{\partial^2 F}{\partial x\, \partial y}\frac{\partial^2 w}{\partial x\, \partial y}\right\}$$

where F is a stress function defined by:

$$N_x = t\frac{\partial^2 F}{\partial y^2}, \quad N_y = t\frac{\partial^2 F}{\partial x^2}, \quad N_{xy} = -t\frac{\partial^2 F}{\partial x \partial y}$$

Modified for the condition of the lateral loading $q = 0$, and for thermal strain, the von Karman equations (4.3.1) become:[6]

$$\nabla^4 F = -\nabla^2 E\alpha T + E\left\{\left(\frac{\partial^2 w}{\partial x \partial y}\right)^2 - \frac{\partial^2 w}{\partial x^2}\frac{\partial^2 w}{\partial y^2}\right\}$$

$$\nabla^4 w = \frac{t}{D}\left\{\frac{\partial^2 F}{\partial y^2}\frac{\partial^2 w}{\partial x^2} + \frac{\partial^2 F}{\partial x^2}\frac{\partial^2 w}{\partial y^2} - 2\frac{\partial^2 F}{\partial x \partial y}\frac{\partial^2 w}{\partial x \partial y}\right\} \tag{4.3.2}$$

In polar coordinates, for axisymmetric conditions, (4.3.2) becomes:

$$\left(\frac{D}{t}\right)\nabla^4 w = \frac{1}{r}\frac{d}{dr}\left(\frac{dF}{dr}\frac{dw}{dr}\right)$$

$$\nabla^2(\nabla^2 F + E\alpha T) + E\frac{1}{r}\frac{dw}{dr}\frac{d^2 w}{dr^2} = 0$$

which may be written:

$$\frac{1}{r}\frac{d}{dr}\left\{r\frac{d}{dr}(\nabla^2 F + E\alpha T)\right\} + \frac{E}{r}\frac{d}{dr}\left\{\frac{1}{2}\left(\frac{dw}{dr}\right)^2\right\} = 0$$

$$\frac{1}{r}\frac{d}{dr}\left\{\frac{dF}{dr}\frac{dw}{dr}\right\} - \frac{D}{t}\frac{1}{r}\frac{d}{dr}\left\{r\frac{d}{dr}(\nabla^2 w)\right\} = 0 \tag{4.3.3}$$

Integrating (4.3.3):

$$r\frac{d}{dr}(\sigma_r r + E\alpha T) + \frac{E}{2}\left(\frac{dw}{dr}\right)^2 = C_1$$

$$\frac{dF}{dr}\frac{dw}{dr} - \frac{E}{2}r\frac{d}{dr}(\sigma_r w) = C_2 \qquad (4.3.4)$$

The constants C_1 and C_2 are zero from the boundary conditions at the center:

$$\phi = \frac{dw}{dr} = 0 \qquad \text{at} \quad r = 0$$

Equation (4.3.4) may be reduced in order by substituting:

$$\phi = \frac{dw}{dr}$$

$$\sigma_r = \frac{1}{r}\frac{dF}{dr}$$

The resulting system of equations is then:

$$\frac{d}{dr}\left\{\frac{1}{r}\frac{d}{dr}(r^2\sigma_r) + E\alpha T\right\} + \frac{1}{2}E\frac{\phi^2}{r} = 0$$

$$\frac{d}{dr}\left\{\frac{1}{r}\frac{d}{dr}(r\phi)\right\} - \frac{1}{b}\sigma_r\phi = 0 \qquad (4.3.5)$$

Because of the non-linearity of (4.3.5) a simultaneous solution for both σ_r and ϕ is necessary. Except for the simplest of problems, the solution is difficult, and an approximate solution in series, or by iterative or energy methods is necessary.

For small deflections as is the case at the onset of buckling, the system (4.3.5) reduces to the linear equation:

$$\frac{d}{dr}\left\{\frac{1}{r}\frac{d}{dr}(r\phi)\right\} = \frac{1}{b}\sigma_r\phi \qquad (4.3.6)$$

The following non-dimensionalizing parameters are introduced:

$$\rho = \frac{r}{b}$$

$$\theta(\rho) = \frac{T(\rho)}{T_0} \tag{4.3.7}$$

$$\tau_0 = 12(1-\nu^2)\alpha \frac{b^2}{t^2} T_0$$

Equation (4.2.11) then becomes:

$$\sigma_r = -\alpha E T_0 \theta$$

where

$$\theta = \frac{1}{\rho^2} \int_0^{\rho} \theta\rho \, d\rho + \left(\frac{1+\nu}{1-\nu}\right) \int_0^1 \theta\rho \, d\rho$$

and (4.3.6) may be written:

$$\phi(\rho)'' + \frac{1}{\rho} \phi(\rho)' - \phi(\rho)\left[\frac{1}{\rho^2} - \tau_0 \theta(\rho)\right] = 0 \tag{4.3.8}$$

The boundary conditions for the fixed-edge case are:

$$\phi(0) = 0$$

$$\phi(1) = 0$$

Exact solutions of (4.3.8) for a given temperature distribution are not readily found, and an approximation method must be used.

The approximation method is that of Stodola and Vianello,[7] illustrated below.

If one substitutes in the right-hand side of the differential equation

$$\frac{d^2y}{dx^2} = -\tau y$$

an approximation, $y = y_1$, and integrates, satisfying the boundary conditions of the problem, a solution, $y_2(x)$ will be obtained which contains the parameter, τ, and thus may be written:

$$y_2(x) = \tau f_1(x)$$

If the approximation had been a characteristic function, the corresponding characteristic value of τ would be given by:

$$\tau_1 = \frac{y_1(x)}{f_1(x)}$$

The first approximation, $y_1(x)$ will in general not give a constant ratio. If $y_2(x)$ is taken as the improved approximation and the cycle repeated, it can be shown that the ratio $y_n(x)/f_n(x)$ tends to a constant value in the interval as n is increased; and that this constant value is the lowest characteristic value, τ.

Successive estimates of the characteristic value after each cycle may be obtained by requiring that the function $y_n(x)$ and $y_{n+1}(x) = \tau f_n(x)$ agree in some sense over the interval, such as given by:

$$T_n = \frac{\int_a^b y_n(x)dx}{\int_a^b f_n(x)dx}$$

The method is applicable to other types of differential equations, such as:

$$\frac{d}{dx}\left[p(x)\frac{dy}{dx}\right] + rr(x)y = 0$$

and

$$\frac{d^2}{dx^2}\left[p(x)\frac{d^2y}{dx^2}\right] + Tr(x)y = 0$$

The detailed solution of (4.3.8) by the Stodola-Vianello method, applied to experimental data, is given in Appendix II.

V. ANALYSIS AND CONCLUSIONS

5.1 Comparison of Experimental Results with Theoretical Critical Temperatures

From Table I the experimental buckling temperature for Run 5/512, the steel plate, is 53.2°F, compared with 54.5°F as calculated in Appendix II. For the aluminum plate, Run 5/508, the experimental value is 28.4°F, compared with the theoretical value of 28.2°F. Considering the many assumptions leading to the approximate theoretical values, the result for the steel plate is reasonably good. The results for the aluminum plate, on the other hand, are not close.

There are several possibilities which may account for the discrepancies. One of these is the lack of initial flatness, or initial curvature of the specimens. It is known that small plate curvatures can cause buckling under edge compressive forces in the (x,y) plane alone.[3] If the initial deflection is w_o, small in comparison with the thickness, and if the subsequent deflection is w_1, equation (4.3.1) becomes:

$$\nabla^4 w_1 = \frac{t}{D}\left[\frac{u}{t} + \frac{\partial^2 F}{\partial y^2}\frac{\partial^2}{\partial x^2}(w_o + w_1) + \frac{\partial^2 F}{\partial x^2}\frac{\partial^2}{\partial y^2}(w_o + w_1)\right.$$

$$\left. - 2\frac{\partial^2 F}{\partial x\,\partial y}\frac{\partial^2}{\partial x\,\partial y}(w_o + w_1)\right] \qquad (5.1.1)$$

From (5.1.1) it is seen that the effect of initial curvature is that of a distributed load:

$$q_o = \frac{\partial^2 F}{\partial y^2}\frac{\partial^2 w_o}{\partial x^2} + \frac{\partial^2 F}{\partial x^2}\frac{\partial^2 w_o}{\partial y^2} - 2\frac{\partial^2 F}{\partial x\,\partial y}\frac{\partial^2 w_o}{\partial x\,\partial y}$$

The compressed plate is analogous to the case of the initially curved compressed bar, and hence the method of Southwell[9] may be used to find the critical temperature should the effects of the initial curvature be large, as they apparently were in the case of the aluminum plate. From a plot of $\frac{w_m}{T_o}$ vs. w_o, the inverse slope of the curve gives $T_{o_{crit}}$. No deflection data were taken in the experiments performed, but this information may be obtained by the optical system used to determine buckling.

Kaliher and Lederman[10] in experimental investigation of thermal buckling of wing cover plates, found that the requirement of perfect flatness is very critical for the validity of the buckling criterion. They found, for instance, that spotwelding of thermocouples to the cover plate produced sufficient initial deviations from flatness to cause the disappearance of the classical buckling phenomenon. The deflections increased gradually from the time heating began.

The plates were inspected carefully for defects and flatness by the optical system. The thermocouples were subsequently located on the plates, and that portion of the plate became "blind" to further inspection since the thermocouples created optical interference. It is possible, then, that spotwelding the thermocouples to the softer aluminum plate created sufficient local deviation from flatness to seriously affect the results.

Part of the discrepancy between experimental and theoretical results may be due to the basic assumption of zero temperature gradient over the thickness being invalid. This possibility is more likely for the aluminum plate, where the buckling time was 22 seconds, compared with 100 seconds for the steel plate. Such a temperature gradient would result in buckling occurring sooner.

In addition, since the thermocouples were located on the opposite side from the heat source, any gradient existing would result in the recording of temperatures lower than the average through the thickness.

5.2 The Buckling Parameter, τ_o

If the shape of the temperature distribution curve is known either from experimental measurement or heat flow theory, the critical buckling temperature may be found for plates of varying material and dimensions by the following method.

Solution of the buckling equation by the method outlined in Appendix II was based on an approximation of the non-dimensionalized temperature distribution, $\theta = T/T_o$, by a second-degree curve:

$$\theta = \alpha\rho^2 + b\rho + c \qquad (5.2.1)$$

From the conditions:

$$\left.\begin{matrix} \rho = 0 \\ \theta = 1 \end{matrix}\right\}, \quad c = 1$$

$$\left.\begin{matrix} \rho = 1 \\ \theta = 0 \end{matrix}\right\}, \quad b = -(a+1)$$

Then (5.2.1) may be written:

$$\theta = a\rho^2 - (a+1)\rho + 1$$

The buckling parameter, τ_o, may be found as in Appendix II, but generalized in terms of a, the experimental curve coefficient. The differential equation (II-1) becomes:

$$\frac{d}{d\rho}\left[\frac{1}{\rho}\frac{d\Psi_2}{d\rho}\right] = -\tau_0\left\{\left[\frac{1}{2}-\left(\frac{7}{12}\right)a+\frac{1}{3}\right]\rho+\left[-\frac{(a+2)}{3}-\frac{1}{\rho}+\left(\frac{7}{12}\right)a\right.\right.$$

$$\left.\left.-\frac{K}{3}\right]\rho^2+\left[\left(\frac{7}{12}\right)a+\frac{1}{3}\right]\rho^3-\left(\frac{a}{4}\right)\rho^4\right\} \qquad \text{where } K=\frac{1+\nu}{1-\nu}$$

With the method given in Appendix II, the first approximation for the buckling parameter is:

$$\tau_0 = \frac{85.3333}{-3.5\,(0.1)+1.3\,(0.3)a} \quad \text{(steel plate)}$$

$$\tau_0 = \frac{22.2222}{-3.57\,(0.1)+1.33\,(0.3)a} \quad \text{(aluminum plate)}$$

Higher accuracy may be obtained by continuing the iteration. On Fig. 13 are shown curves of τ_0 vs. a for steel and aluminum for the range of temperature distribution curves given in Fig. 14.

One may estimate critical temperature as follows: On Fig. 14 plot the experimental or theoretically derived distribution curve, to obtain a value of a. From Fig. 13 obtain the buckling parameter, τ_0. The estimate of the critical temperature is then known from (4.3.7).

5.3 Conclusions

The low experimental buckling temperatures observed in this investigation are likely the result of initial curvature effects.

It is possible, knowing the temperature distribution experimentally or from heat flow theory, to predict the buckling temperature by a plot of the buckling parameter, τ_0, vs. a temperature shape coefficient, as given in Fig. 13.

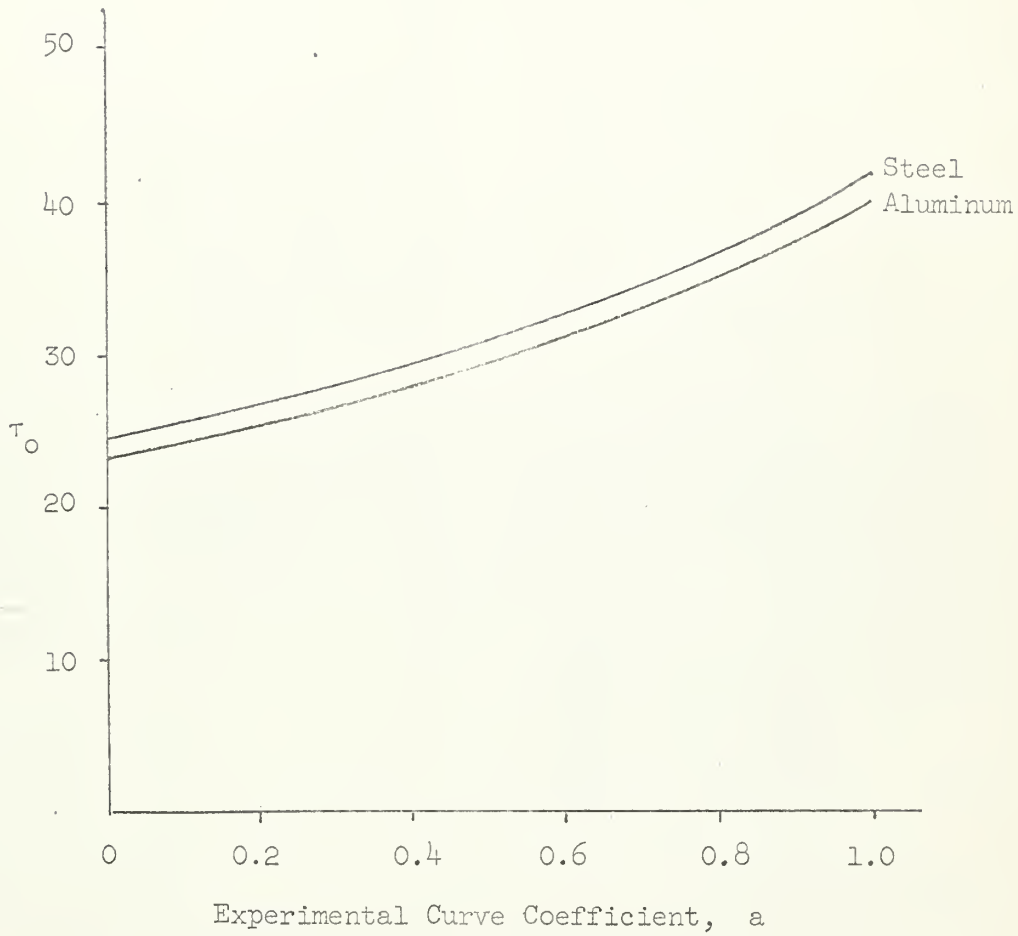

Fig. 13 Buckling Parameter-Temperature Distribution Plot

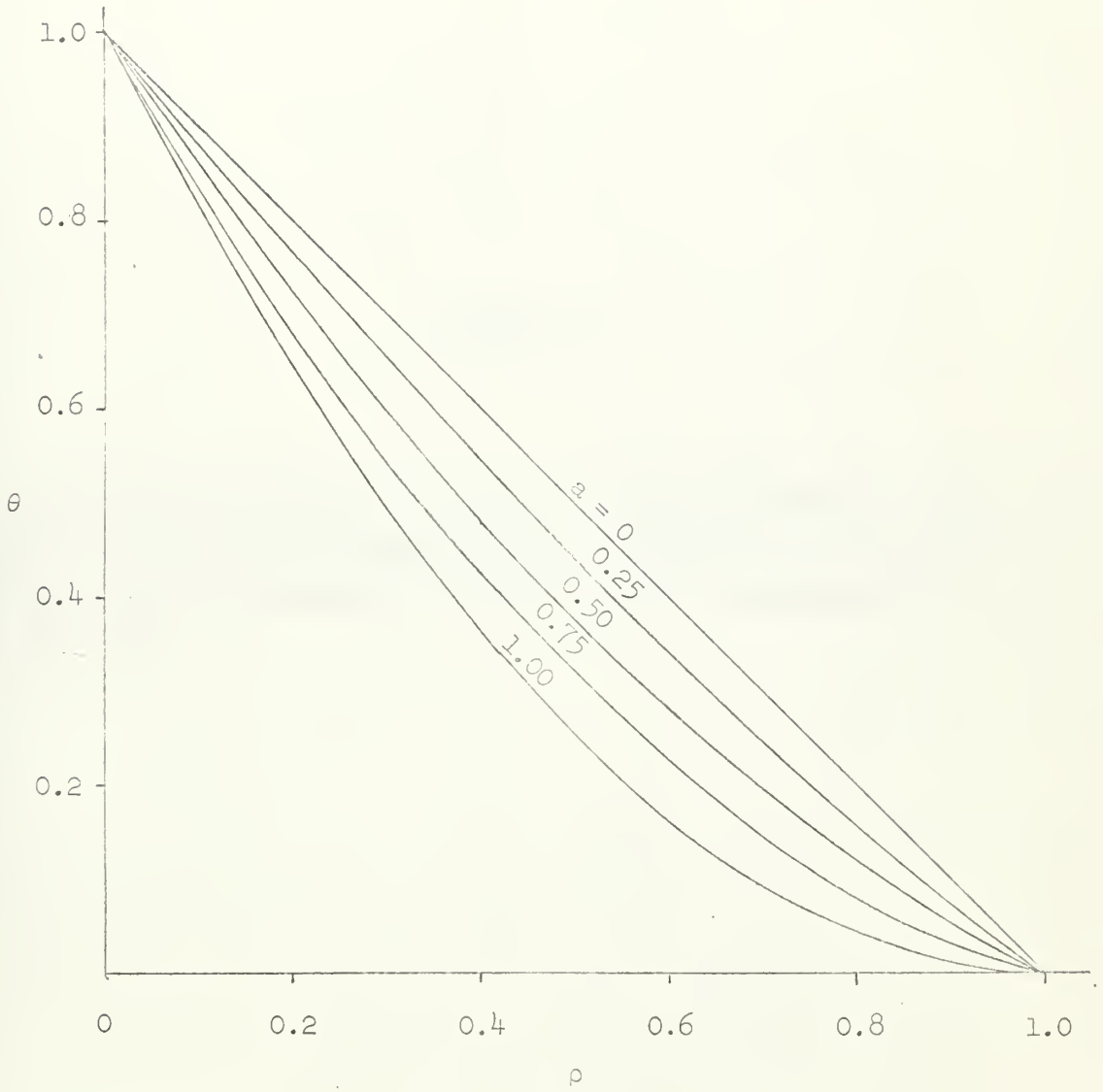

Fig. 14 Temperature Distribution Curves

APPENDIX I

This Appendix is a reproduction of a paper presented to the Eleventh Annual Western Region Student Conference of the Institute of the Aerospace Sciences, held in Los Angeles, California on May 12, 1961.

AN OPTICAL METHOD FOR THE DETERMINATION OF BUCKLING DEFLECTIONS

by

Lt.Col. W. B. Higgins, USMC

and

Lt. D. W. Mathews, USN

Stanford University
Stanford, California

INTRODUCTION

Success in experimental research depends upon the ability to measure length, time, and mass with precision. Thus over the years, much thought has been devoted by experimentalists to techniques for determining these quantities. Optical methods have long been accepted as the most precise for the determination of the flatness or shape of an object. Therefore, all engineers are acquainted with the principles of interferometery, the diffraction grating and the use of the optical comparator.

The structural problem with which we have been concerned is the determination of time of buckling and mode, in a plate heated in its center. It is clear, in a problem of this kind, that the means of measurement should not influence the results of the experiment.

Thus in our planning, many kinds of transducers or methods were considered, but in each case we found that there was an inter-action between transducer and the plate. Among the types of transducers we considered were: capacity type, gages, variable reluctance pick-ups and

---

The research outlined in this paper was sponsored by the United States Air Force under contract no. AF49(638)-223, and was carried out in the Department of Aeronautical Engineering at Stanford University under the direction of Professor W. H. Horton.

also linear potentiometers. They were all discarded in favor of an optical method. Clearly, a straight modification of the basic interferometric principle used for the determination of flatness is not possible, because the heat would cause the optical flats normally used on this type of work, to distort and so would interfere with our results. But the "Moire" pattern to be described in this paper does not have this disadvantage, nor indeed does it in any way interfere with the problem.

As we shall show, the method is extremely simple, accurate, low in cost, and readily available in any research laboratory. Indeed, the phenomenon has been observed by us all, usually without appreciating its significance. Most of us have noticed that the overlapping of two lattices of nearly equal mesh produces visible fringe patterns when viewed against a light background. Because this effect is merely mechanical, and is not related to the nature of the light employed, it is convenient to refer to it as mechanical interference. It is the purpose of this paper, to investigate the possible uses of this phenomenon in connection with the determination of the buckling of plates.

GENERAL

When a uniform set of parallel lines, produced on a transparent material, is superposed on another set of identical lines and moved in a direction normal to them, we get alternate light and dark lines (fig.1). This variation is produced as the two sets of lines alternately overlap and interlap and is strictly a mechanical effect. If the spacing of one set of lines differs slightly from the other, the alternate areas of light and dark occur without relative movement (fig.2). The dark areas parallel to the lines are interference fringes.

Fringes are also visible when a set of parallel lines, produced on a transparent material, is superposed on another set of parallel lines at a slight angle (fig.3). The greater the angle between the sets of lines, up to a limit of ninety degrees, the greater the number of fringes.

Fig. 1

Fig. 2

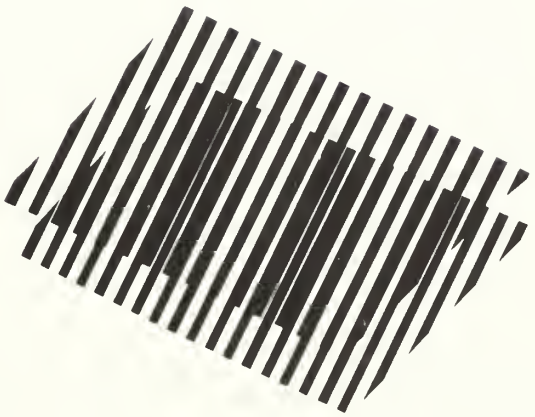

Fig. 3

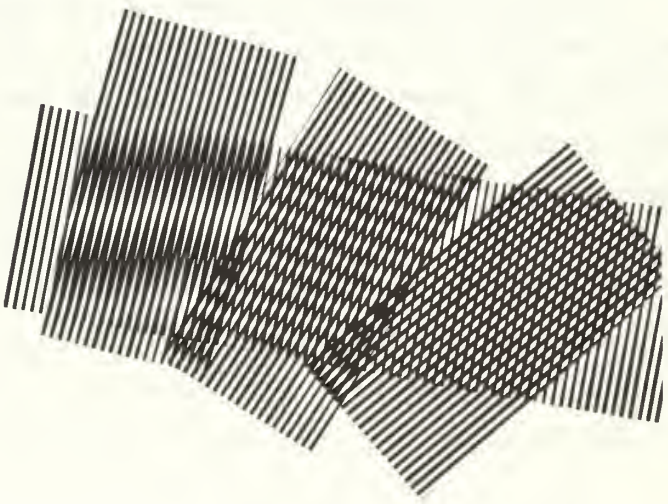

FRINGE PHENOMENON

For small angles, the fringes are at almost right angles to the lines. The relation being given as $90^{\circ} \pm \frac{\beta}{2}$ where β is the angle between the sets of lines. If h is the line spacing, the fringe spacing is $\frac{h}{2}$ cosecant $\frac{\beta}{2}$. This type of mechanical interference is known as "Moire" fringes; the name coming from the French and meaning: "having a wavelike pattern".

The physics of the method is extremely simple, it is nothing more than the reflection of a ray of light from a surface (fig.4). The change in angle of reflection is twice the change in angle of the reflecting surface. If the deflection of a reflected light ray is measured at a known distance, the change in slope of the surface can be calculated from geometry. As a simple expedient in bookkeeping of the rays, we use movement in one direction and alternate the color of the rays in that direction. In our case we use alternating black and white parallel lines. Sensitivity of the system can be increased by measuring movement of the associated "Moire" fringes. The sensitivity is directly proportional to the cotangent of the angle of rotation between the two sets of superposed lines.

The method is not new. It was first reported in 1948 by Weller and Shepard of the Naval Ordnance Laboratory, Washington, D.C. Their short paper described some of the possibilities of the method. It was followed in 1955 by a paper given by Ligtenberg from the Technological University of Delft. This paper was titled "The Moire Method - A New Experimental Method for the Determination of Moments in Small Slab Models". Ligtenberg placed a model with a mirror surface in front of a circular screen on which was ruled six lines per inch. From the center of the back of the screen, he viewed the reflected lines shown in the mirrored surface. Using a camera, he recorded the initial position of the reflected lines. The model was then loaded in such a manner that the deflections were normal to the screen and hence the change in slopes of the model surface caused the reflected lines to appear in a different position. A second exposure was superposed on the same film and consequently after development, "Moire" fringes appeared. From geometry, slopes of the model were calculated.

LIGHT RAY REFLECTION

Fig. 4

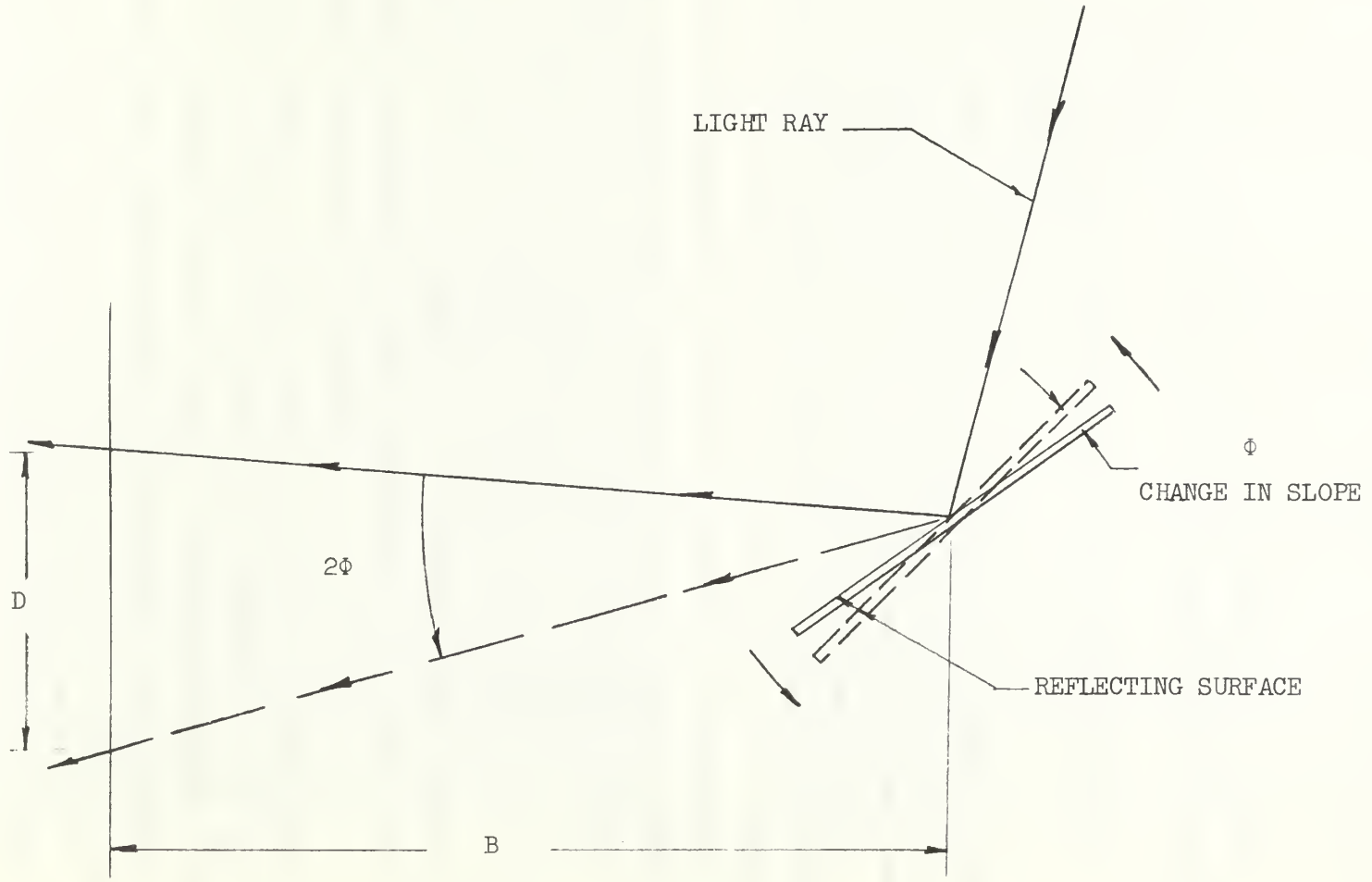

DEVELOPMENT

In order to develop a satisfactory procedure for measuring buckling deflections in the thermal stress problem, work was divided into three stages:

1. Development of the basic optical and photographic techniques.
2. Application of the techniques to a flat plate simply supported on two edges.
3. Actual application to the thermal stress problem involving a thin disc.

The first stage: A polaroid land camera was used to make a lantern slide transparency of a set of ruled parallel lines. Line and spacing width was one-sixteenth of an inch. A 35 mm slide made from the transparency was projected on a 10 × 12 inch alzac test surface with a La Belle 500 projector. The image of the lines was reflected from the test surface to a 20 × 20 × 1/8 inch milk glass focusing plate. The optics and equipment were symmetrically placed with respect to a horizontal plane, with the parallel lines and supporting edges of the test plate also horizontal (fig.5). This orientation provided maximum intensity and contrast because of the surface condition of the test plate. In manufacture of the alzac, minute scratches were made on the surface in line with the direction of rolling. These caused diffusion of the reflected light. With the projected lines oriented at right angles to the scratches, the diffusion of light reinforced the lines and hence intensity and contrast were at a maximum.

The second system of parallel lines was formed by placing paper strips across the back side of the milk glass, inclined by about ten degrees to the reflected horizontal lines. The optical distance of five feet produced lines of approximately three-sixteenths of an inch wide. Intensities of the two sets of lines were matched by varying the density of the paper strips. The "Moire" fringe lines which appeared on the milk glass were successfully photographed with a Speed Graphic Camera (fig.6).

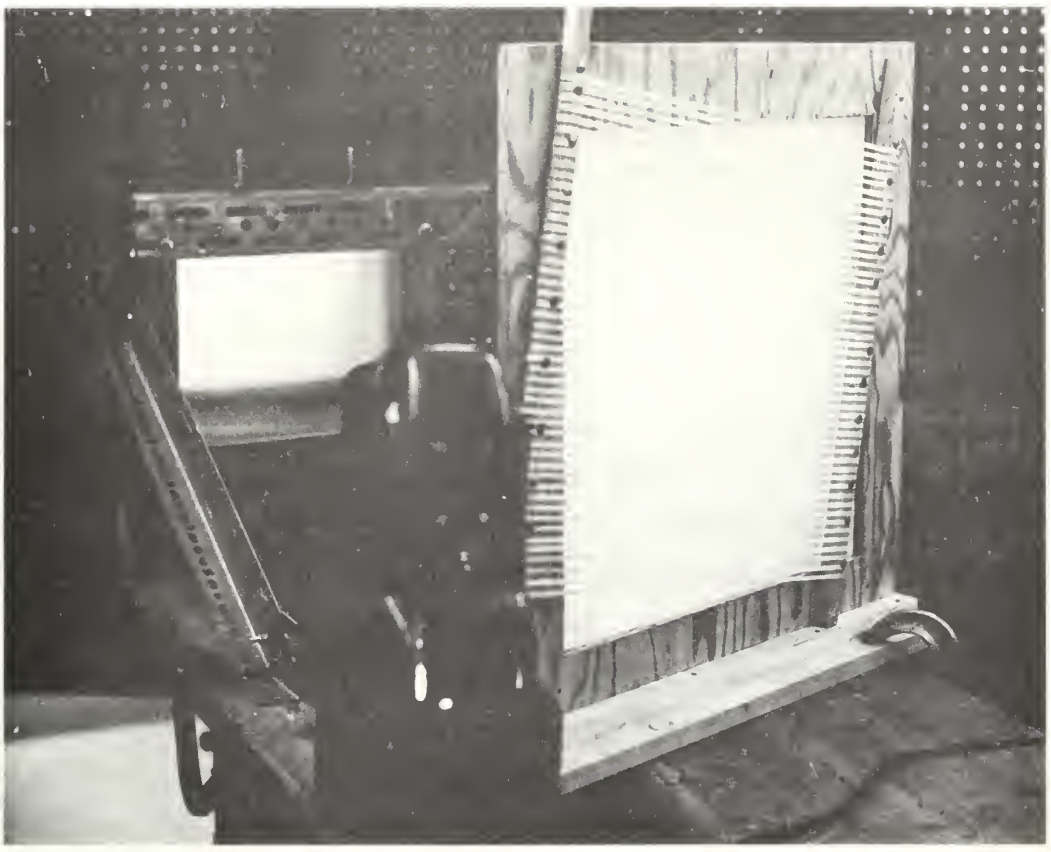

Fig.5 FIRST STAGE APPARATUS

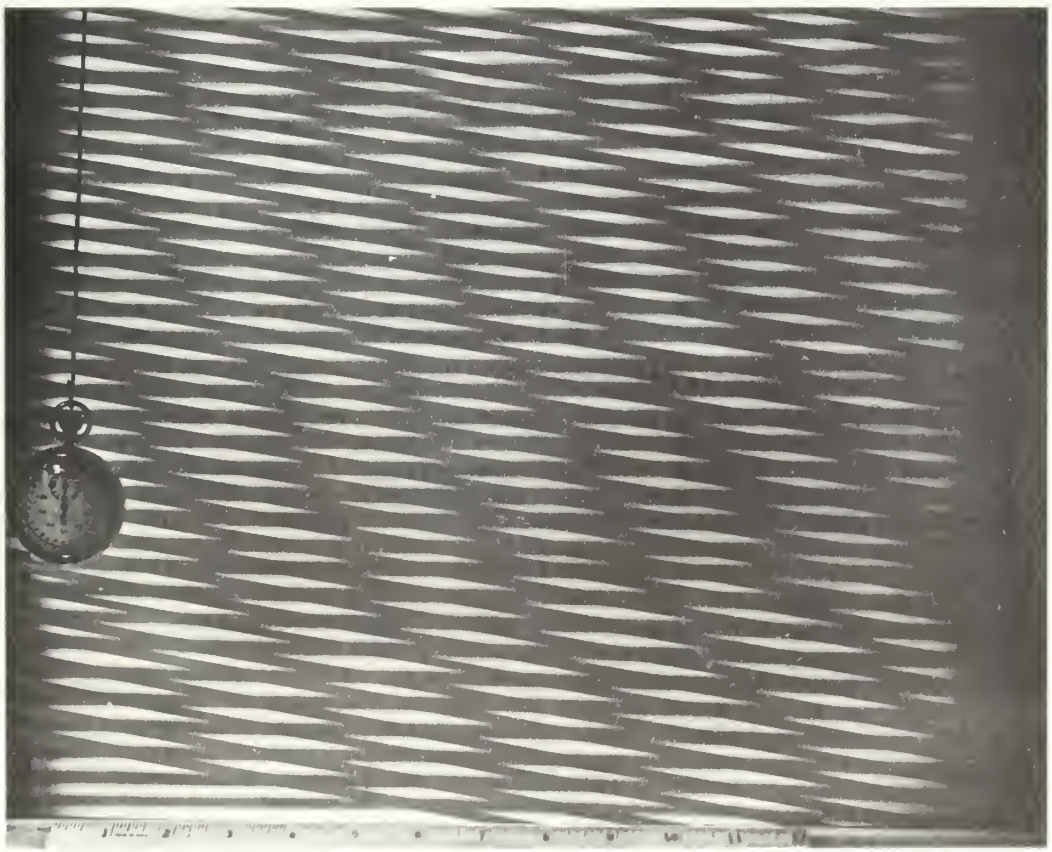

Fig.6 FIRST STAGE FRINGE PATTERN

It was found that the accuracy of the line spacing was most important in order to produce smooth fringes. Drafting tools were used to rule the set of lines photographed in this test, but the uniformity of spacing was not the best. It was also found that more lines per inch were necessary to eliminate the jagged appearance of the fringes.

In the second stage, the geometry of the optics in the simply supported plate problem was as shown in figure 7. Two assumptions were made in our analysis. Delta is much less than B and $\tan 2\Phi$ is much less than one. Since the deflection of the plate is of the order of one-tenth of an inch and B is of the order thirty inches, delta can be neglected. The movement of the projected lines on the focusing plate is a function of the angle α, which varies for each line. The angle α corresponding to any projected line can be obtained from geometry. The maximum value for $\tan \alpha$ is 0.15 and for fringe movements up to about 25 inches, the error in assuming $\tan \alpha \tan 2\Phi$ equal to zero is less than 1%. Therefore, the equation reduces to $D = B \tan 2\Phi$ and a solution for the slope Φ for any observed line displacement is obtainable.

One main advantage of this method of measurement lies in the sensitivity which is gained by measurement of the relatively large movement of the fringe Γ for small movement of the reflected line D. The slope at a distance x from the origin is therefore determined from the equation $\tan 2\Phi = \frac{\Gamma}{B} \tan \beta$.

To demonstrate the sensitivity, three central deflections were used at the one-quarter point of the test specimen. The angle between the sets of lines being 10 degrees. For a central deflection of one-tenth of an inch, the fringe movement corresponding to the change in slope at the one-quarter point was 7 inches. For a deflection of one one-hundredth, the fringe movement was approximately three quarters, and a one one-thousandth, a sixteenth. The high sensitivity achieved with this method is evident.

The development is now in the third stage and is based on the following proposal (fig.8). In the actual experiment, temperature and deflection will be recorded versus time from the instant the heat source is turned on until thermal equilibrium is reached. A motion picture camera will be

GEOMETRY

Fig. 7

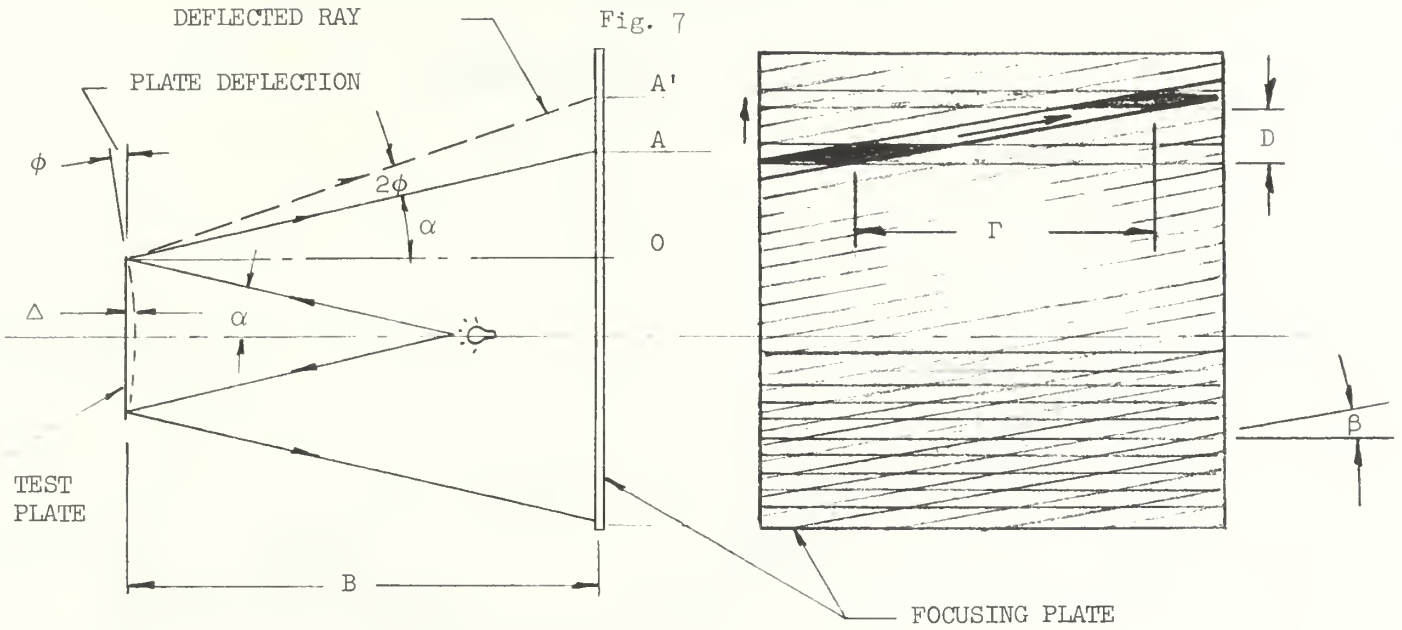

FROM GEOMETRY: $D = OA' - OA = (B - \Delta)[\tan(2\phi + \alpha)] - B \tan \alpha$

$$= (B - \Delta)\left[\frac{\tan 2\phi + \tan \alpha}{1 - \tan \alpha \tan 2\phi}\right] - B \tan \alpha$$

ASSUMPTIONS: 1. $\Delta \ll B$, 2. $\tan \alpha \tan 2\phi \ll 1$

THEREFORE: $D = B \tan 2\phi$ BUT $\tan \beta = D/\Gamma$

THEREFORE:

$$\tan 2\phi_x = \frac{\Gamma_x}{B} \tan \beta$$

PROPOSED SYSTEM

Fig. 8

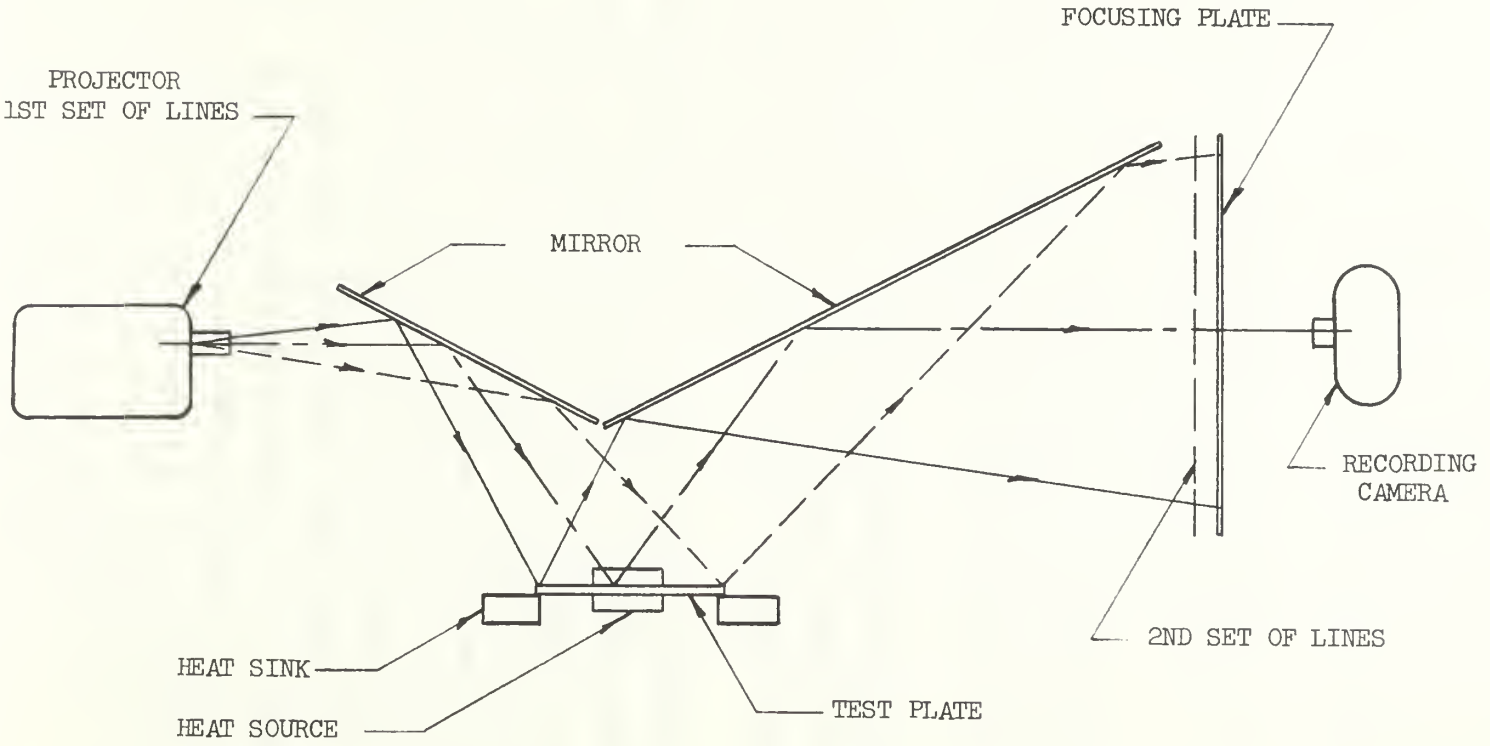

used to record changing position of the fringes. A stop watch and scales will be included in the photograph to indicate the time on each frame of the film and establish the magnitude of fringe movement. The determination of time of initial buckling is simply determined by noting when movement of the fringe is apparent in the developed film. The actual movement of the fringes can be read by enlarging the appropriate frame for any given time, to a convenient size.

In testing the thermally stressed disc, it was desired to mount the disc in a horizontal position, therefore, two plate glass mirrors were used to reflect the light rays to a more convenient position.

In preparing the slides for the final test, it was found that cellophane tape was available in widths of one-sixteenth of an inch and larger and in a variety of colors. The tape is sold under the trade name of Applied Graphics Corporation Drafting Tape.

A very precise set of parallel lines was constructed using three thirty-seconds tape, on frosted glass. This width was convenient to work with and the glass made it easy to adjust the tape. The use of tape also gave maximum definition to the line edge.

One of the problems with the earlier black and white lines was locating on the focusing plate, a point corresponding to a specific point on the test surface. A particular line could be traced through the optical system but because of the nature of the pattern, the lines soon begin to interchange and were difficult to follow. The new set was made using colored lines alternating black, green, red and blue. The lines, laid out in a fifteen inch square on the frosted glass, were photographed with a speed graphic camera using strobe illumination. The second set of lines was constructed with a spacing of thirty-six lines per foot by making a positive from a black and white negative. DuPont "Cronar", a dimensionally stable, high contrast litho film was used for the positive and is available in 22 × 29 inch sheets. The positive was sprayed with "Quik-Stick", a spray adhesive, on the emulsion side and simply stuck to the two and one-half foot square milk glass focusing plate.

A LaBelle 500 projector is used to project the two by two slides oriented with the lines vertical, to eliminate problems caused by the double image from the first surface of the mirror. In other words, the lines are simply reinforced by their own image.

The set of lines is reflected from the first mirror to the reflecting surface of the alzac test disc, then to the second mirror and finally through the second set of lines onto the milk glass. From the opposite side of the focusing plate, the individual lines and "Moire" fringes are clearly visible. Figure 9 illustrates the fringe pattern before buckling and figure 10 shows the fringes after buckling. The figures were taken from a 16 mm movie of a test run. The fringe movement is converted to slope using the derived formula and deflection obtained by graphical integration of the slope function.

CONCLUSIONS

In conclusion I would like to say, while further development is clearly required, we believe that this presentation of the "Moire" method has demonstrated that it is possible to determine the time of buckling of a loaded body with precision, that it is feasible to determine the mode of buckling over a relatively large area and that the equipment needed for such investigation is simple, inexpensive and readily available. Since contact with the object under investigation is totally unnecessary, the method can be applied in cases in which environmental conditions or interaction problems make the use of normal instrumentation either extremely difficult or not applicable.

It is important to point out that changes in deflection are derived from changes in slope, and therefore the technique is not restricted to initially plane surfaces or unloaded specimens.

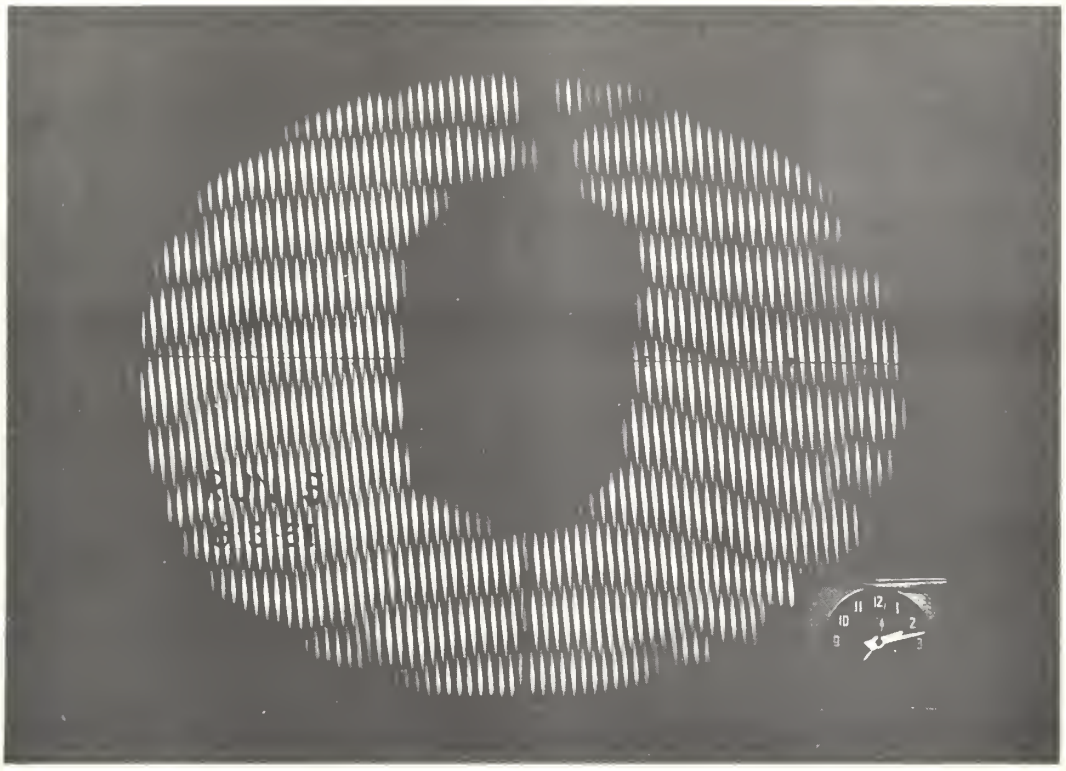

Fig.9 FRINGE PATTERN BEFORE BUCKLING

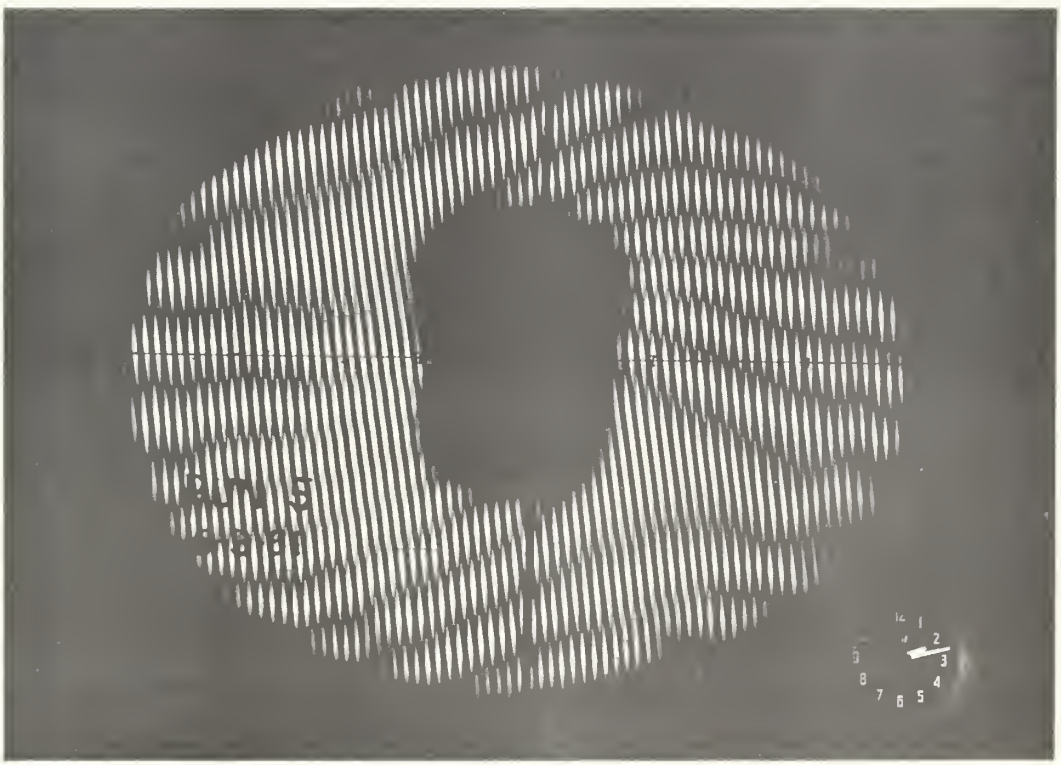

Fig.10 FRINGE PATTERN AFTER BUCKLING

BIBLIOGRAPHY

1. Displacement Measurement by Mechanical Interferometry, Weller, R., and Shepard, B. M., Society of Experimental Stress Analysis Proceedings, Vol.6, No.1.

2. The Moire Method - A New Experimental Method for the Determination of Moments in Small Slab Models, Ligtenberg, F. K., Society of Experimental Stress Analysis Proceedings, Vol.12, No.2.

APPENDIX II

CALCULATION OF THEORETICAL CRITICAL TEMPERATURE USING THE VIANELLO-STODOLA METHOD AND EXPERIMENTAL DATA.

The equation for small deflections:

$$\phi(\rho)'' + \frac{1}{\rho}\phi(\rho)' - \phi(\rho)\left[\frac{1}{\rho^2} - \tau_0 \theta(\rho)\right] = 0 \qquad (A.3.3)$$

may be written:

$$\frac{d}{d\rho}\left\{\frac{1}{\rho}\frac{d}{d\rho}(\rho\phi)\right\} = -\tau_0 \theta\phi$$

A change of variables may be made, giving:

$$\frac{d}{d\rho}\left\{\frac{1}{\rho}\frac{dy}{d\rho}\right\} = -\tau_0 r(\rho) y \qquad (II\text{-}1)$$

where

$$\frac{\theta(\rho)}{\rho} = r(\rho)\ , \qquad \phi(\rho)\cdot\rho = y$$

To satisfy the boundary conditions on y, the first approximation is taken as:

$$y = y_1 = (\rho - \rho^2)\rho = \rho^2 - \rho^3 \qquad (II\text{-}2)$$

$$y(0) = \phi(0)\cdot 0 = 0$$

$$y(1) = \phi(1)\cdot 1 = 0$$

Before integrating (II-1), an approximate analytic value for the stress parameter, ϕ, is required, which in turn leads to an approximation for the temperature distribution parameter, θ. Fitting a curve to the temperature distribution plot for Run 59512 (steel plate) gives the following approximation:

$$\theta = 0.625\rho^2 - 1.625\rho + 1 \qquad \text{(II-3)}$$

The experimental plot for Run 59512 and the approximation curve are shown in Fig. II-1.

The stress parameter approximation becomes:

$$\phi(\rho) = \frac{1}{\rho^2}\int_0^{\rho} \theta\rho\, d\rho + \left(\frac{1+\nu}{1-\nu}\right)\int_0^{1} \theta\rho\, d\rho$$

$$= 0.15625\rho^2 - 0.54167\rho + 0.7063$$

Hence:

$$r(\rho)\, y_1(\rho) = \frac{b}{\rho}(\rho^2 - \rho^3) = 0.7063\rho - 1.2604\rho^2$$

$$+ 0.5729167\rho^3 - 0.15625\rho^4$$

Substituting the last expression into the right-hand side of (II-1) and integrating, one obtains:

$$y_2 = -\tau_0\left[+0.0333333\rho^4 - 0.0833333\rho^5 + 0.0290179\rho^6\right.$$

$$\left. - 0.0044643\rho^7 + \frac{C_1}{2}\rho^2 + C_2\right]$$

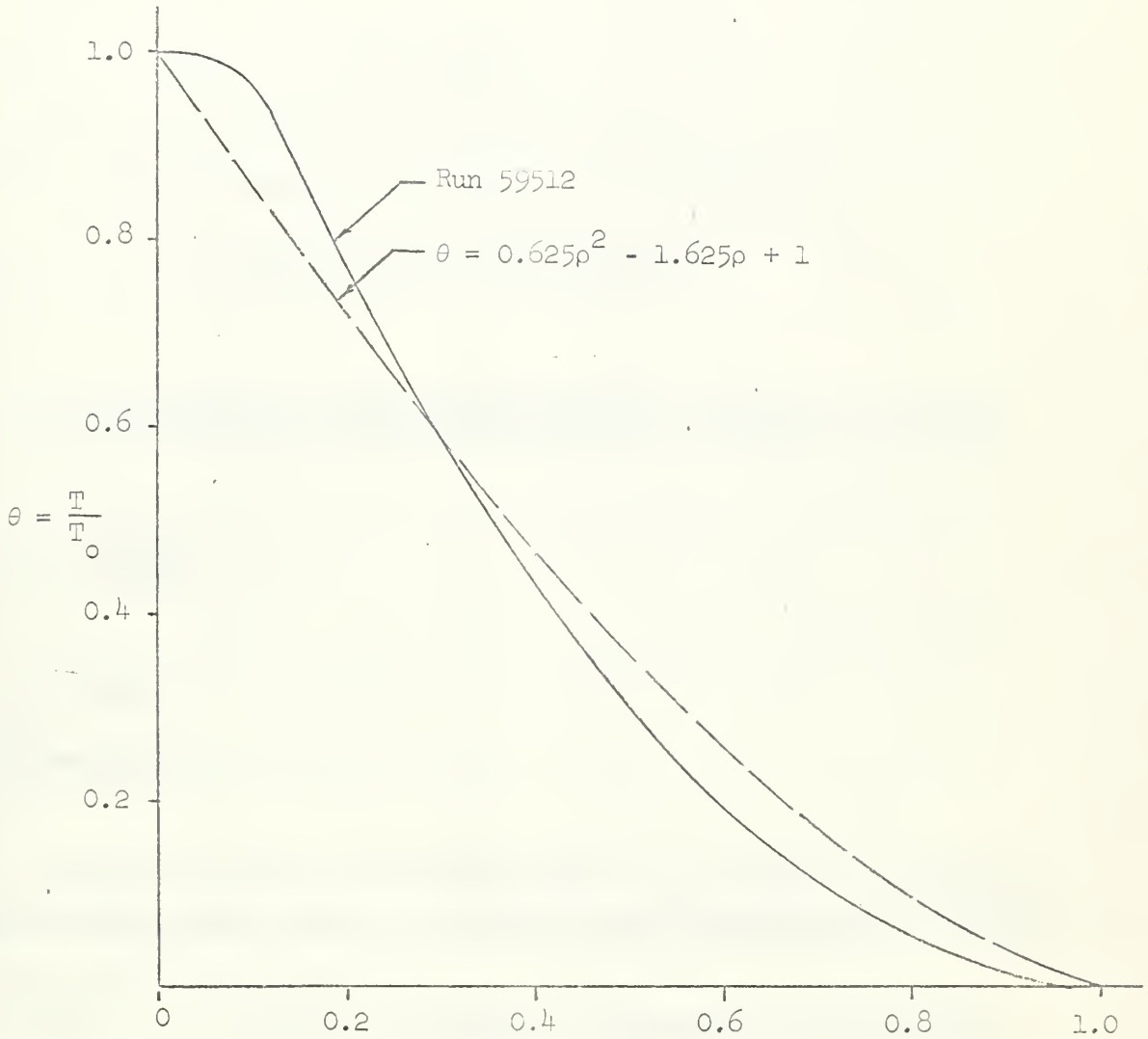

Fig. II-1 Experimental and Approximated Temperature Distribution

From the boundary conditions (II-2), $C_2 = 0$, and $\frac{C_1}{2} = -0.02971023$

The first approximation of the characteristic value is:

$$\tau_{o_1} = \frac{\int_0^1 (\rho^2 - \rho^3)d\rho}{\int_0^1 (+0.0503392\rho^4 - 0.0932826\rho^5 - 0.0290793\rho^6 - 0.0044642\rho^7 - 0.0297102\rho^8)d\rho}$$

$$= \frac{0.033333 \times 10^3}{(+17.\ldots - 13.072105 + 4.154226 - 0.555035 - 0.\ldots)}$$

$$= \frac{33.333}{2.514355}$$

$$\tau_{o_1} = 33.136$$

For the next cycle the expression for f_1, which is a multiple of the last improvement upon y, is used in the right-hand side of (II-1):

$$\frac{d}{d\rho}\left[\frac{1}{\rho}\frac{dy}{d\rho}\right] = -\tau_{o_2}(10^{-3})[-21.0055285 + 14.0973756\rho^2 + 57.7936936\rho^3 - 106.8790008\rho^4 + 79.4410396\rho^5 - 31.9121451\rho^6 + 6.\ldots\rho^7 - 0.6754434\rho^8]$$

Integrating once gives:

$$\frac{1}{\nu}\frac{dy_3}{dx} = -\tau_{o_2}(10^{-3})[-10.\ldots x^4 + 5.\ldots x^5 + 14.\ldots x^6$$

$$- 21.\ldots x^8 + 13.\ldots x^9 - 4.\ldots x^7 + 0.\ldots x^3$$

$$- 0.\ldots x^9 + C_1]$$

A second integration gives:

$$y_3 = -\tau_{o_2}(10^{-3})[-2.\ldots x^4 + 1.\ldots x^5 + 2.\ldots x^6$$

$$- 3.\ldots x^7 + 1.\ldots x^8 - 0.\ldots x^9 + 0.\ldots x^{10}$$

$$- 0.\ldots x^{11} + \frac{C_1}{2}x^2 + C_2]$$

With the boundary conditions evaluated the second approximation for the characteristic value is:

$$\tau_{o_2} = \frac{\int_0^1 f_1 \, db}{\int_0^1 (-2.625[illegible]b^4 + 1.0731[illegible]b^5 + 2.[illegible]b^6 - 3.0479714b^7 + 1.[illegible]b^8 - 0.[illegible]b^9 + 0.[illegible]b^{10} - 0.0070459b^{11} + 0.[illegible])(10^{-3})db}$$

$$= \frac{2.524[illegible]}{(-0.525[illegible] + 0.17335[illegible] + 0.3[illegible] - 0.[illegible] + 0.1[illegible] - 0.0[illegible] + 0.007[illegible] - 0.000[illegible] + 0.[illegible])}$$

$$= \frac{2.524[illegible]}{0.07[illegible]}$$

$$\tau_{o_2} = 32.0[illegible]$$

The second value is 3.2 per cent of the first.

The approximate critical value of the central temperature is obtained from (4.3.7):

$$T_o = \frac{t^2}{12(1-\nu^2)\alpha b^2}\,\tau_{o_2}$$

$$= \frac{(0.074)^2}{12(1 - 0.287^2)(6.1 \times 10^{-6})(5.0)^2}\,(32.07)$$

$$= (3.26)(32.07)$$

$$T_o = 104.5\ ^{\circ}F$$

Partial calculations for Run 57702 (aluminum plate) are given below. The experimental and approximated temperature distribution curves are shown in Fig. II-2.

$$\theta = 0.9\rho^2 - 1.9\rho + 1$$

$$\phi = 0.2250\rho^2 - 0.6353\rho + 0.4334$$

$$y_1 = \rho^2 - \rho^3$$

$$y_2 = -\tau_o(10^{-5})(+ 95.4250000\rho^4 - 87.7800000\rho^5$$

$$+ 35.7625000\rho^6 - 5.4285714\rho^7 - 26.5733920\rho^3)$$

$$\tau_{o_1} = \frac{83.3333}{2.23602} = 37.325$$

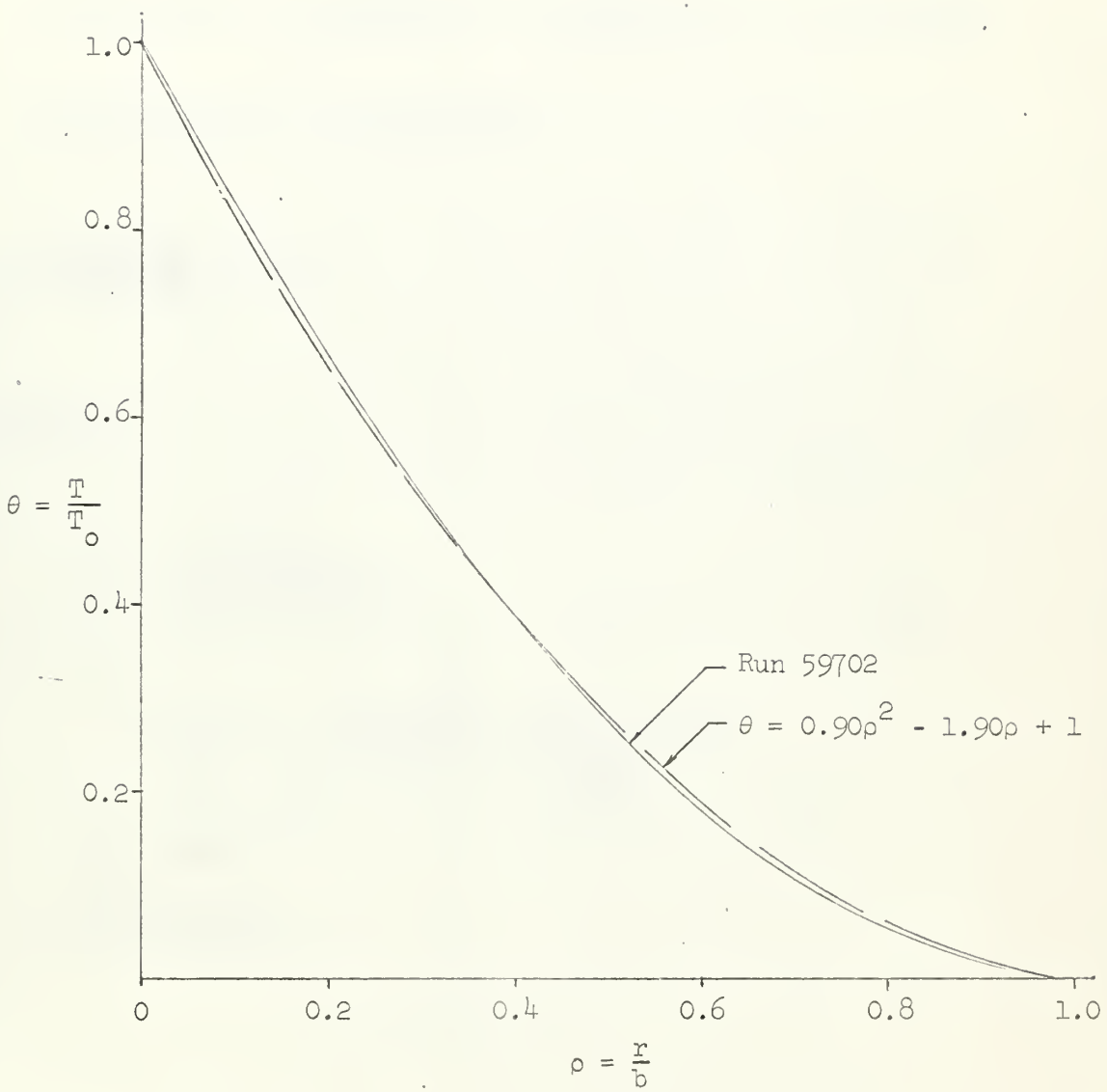

Fig. II-2 Experimental and Approximated Temperature Distribution

$$\gamma_3 = -\tau_c(10^{-3})(-2.304679010p^4 + 1.15709053p^5 + 2.17[illegible]10^4$$

$$- 5.25[illegible]71550p^7 + 2.0077[illegible]4p^8 - 0.7[illegible]p^9 + 0.151[illegible]p^{10}$$

$$- 0.014[illegible]p^{11} + 0.713[illegible]p^2)$$

$$\tau_{o_2} = \frac{2232.8121}{62.1316} = 35.93$$

From which:

$$\tau_{o_2} = \frac{t^2}{12(1-\nu^2)\alpha\beta^2}\,\tau_{o_2}$$

$$= \frac{(0.034)^2}{12(1 - 0.111)(12.3 \times 10^{-6})(25)}\,35.93$$

$$\tau_{o_2} = 43.2\ {}^{o}F$$

APPENDIX III

SAMPLE CALCULATIONS

Temperature reduction for Run 59512 is given in Table II. The calculation is made as follows:

For Thermocouple No. 1, the galvanometer swing at buckling was 1050 Oscillograph Reader Units, which from a calibration graph for that oscillograph channel gives 2.125 millivolts. The ambient temperature of 77°F corresponds to a room temperature reference junction value of 1.000 millivolts. From Leeds and Northrup Company's conversion table for thermocouples, the sum, 3.125 millivolts, gives a temperature of 170.2°F. The temperature rise, T, is then $170.2 - 77.0 = 93.2°F$.

The stress distribution, σ_r, is obtained by a mechanical integration of Equation (4.2.11):

$$\sigma_r = -\frac{\alpha E}{r^2}\int_b^r Tr\,dr - \frac{\alpha E}{r^2}\frac{(1+\nu)}{(1-\nu)}\int_b^b Tr\,dr$$

For the steel plate:

$$\alpha = 6.1 \times 10^{-6}/°F$$

$$E = 30 \times 10^6 \text{ lb/in.}^2$$

$$\nu = 0.287$$

TABLE II

TEMPERATURE REDUCTION, RUN 59512

Thermocouple No.	1	2	3	4	5	6	7	8	9	10	11
Galvanometer No.	1	2	4	3	5	6	7	8	9	10	11
Galvanometer Swing, Scale Units	1090	1028	905		806	654	424	350	148	100	29
Millivolts	2.125	2.070	1.831	Malfunction	1.550	1.160	0.716	0.645	0.391	0.320	0.091
Temperature Corrected to 32°F, Millivolts	3.125	3.070	2.831		2.550	2.160	1.716	1.645	1.391	1.320	1.091
°F	170.2	167.7	157.3		145.0	128.0	108.7	105.7	94.5	91.5	81.0
Temperature Rise, T °F	93.2	90.7	80.3		68.0	51.0	31.7	28.7	17.5	14.5	4.0
Thermocouple Location, inches from center	0	1/2	3/4		1	1 1/2	1 3/4	2 1/4	3	3 1/4	4 1/4

Ambient temperature: 79°F

E_{79} = 1.000 millivolts

Then:

$$\sigma_r = -\frac{183.0}{r^2}\int_0^r Tr\,dr - 13.2\int_0^b Tr\,dr$$

The temperature distribution from Table II is plotted in Fig. III-1 and the product Tr vs. r in Fig. 13.

From Fig. III-2 the second term for σ_r is:

$$-13.2\int_0^b Tr\,dr = -(13.2)(235.5) = -3100$$

For r = 1.5 in., the first term is:

$$-\frac{183.0}{2.25}(31.5) = -6630$$

Then $\sigma_{r_{0.5}} = -9730$ lb/in.^{2}

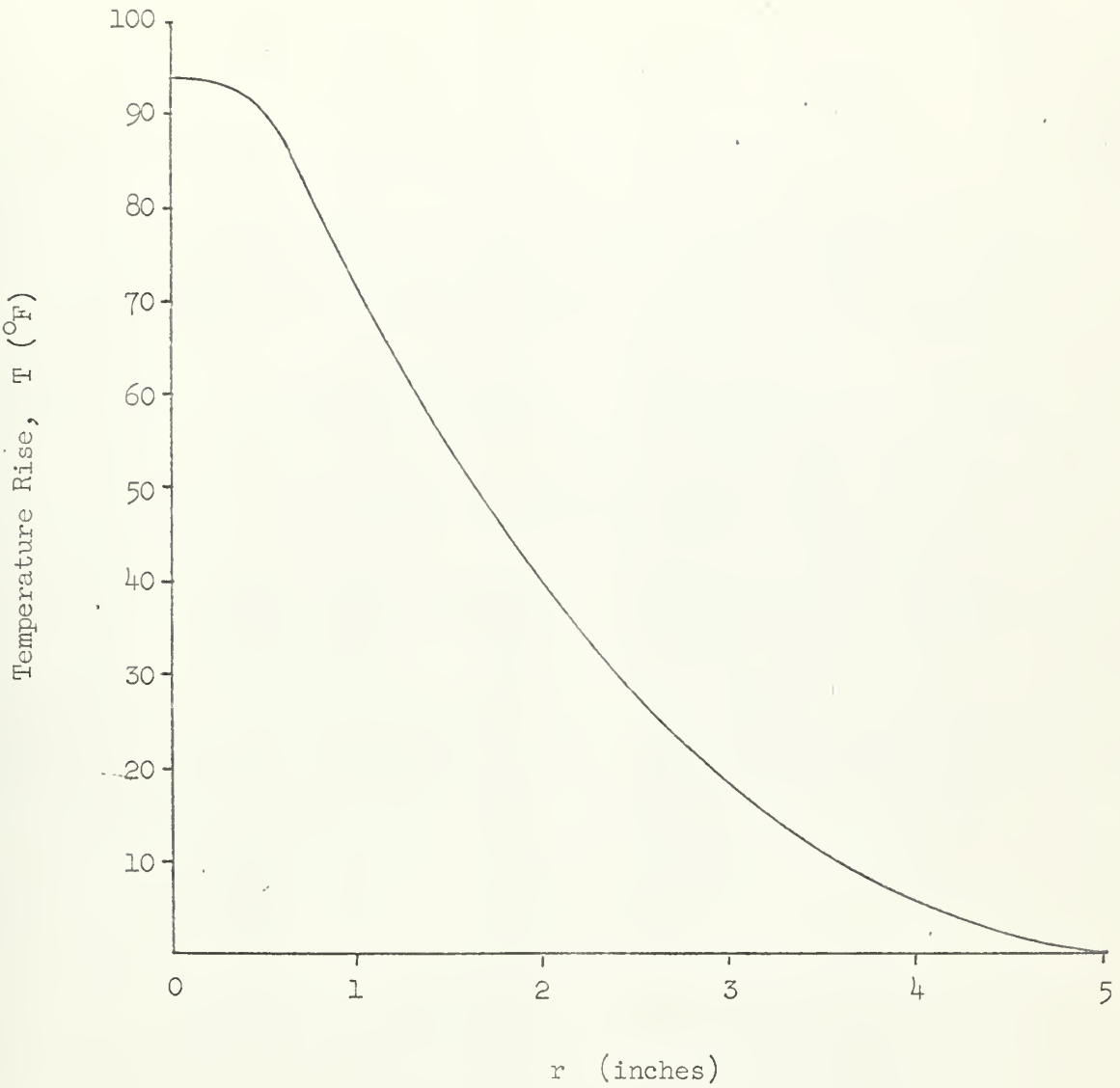

Fig. III-1 Temperature Distribution
(Run 59512)

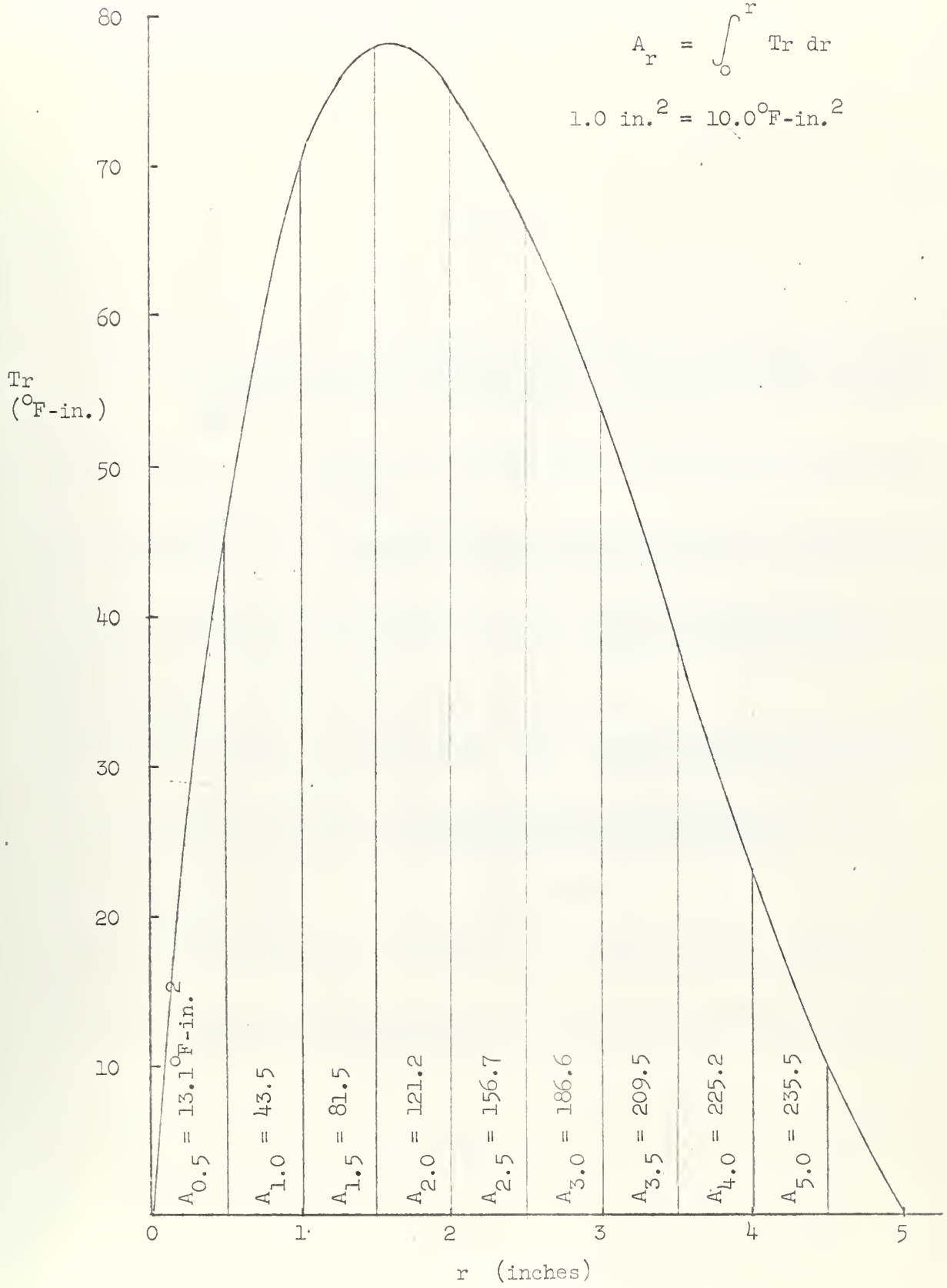

Fig. III-2 Tr vs. r

REFERENCES

1. Duhamel, J. M. C.: "Memoire sur le Calcul des Actions Moleculaires Developpées par les Changements de Temperature dans les Corps Solides", Memoires de l'Institut de France, 5, pp. 440-498, 1838.

2. Wolf, H. J.: "Buckling and Stability", Forty-First Wilbur Wright Memorial Lecture, 1953.

3. Timoshenko, S.: Theory of Elastic Stability, 1st ed., McGraw-Hill Book Co., Inc., New York, 1936, pp. 367-371.

4. Timoshenko, S., and Goodier, J. N.: Theory of Elasticity, 2nd ed., McGraw-Hill Book Co., Inc., New York, 1951, pp. 405-406.

5. Timoshenko, S.: loc. cit., pp. 302-303.

6. Boley, Bruno A., and Weiner, J. H.: Theory of Thermal Stresses, John Wiley and Sons, Inc., New York, 1960, pp. 146-147.

7. Hildebrand, F. B.: Advanced Calculus for Engineers, 1st ed., Prentice-Hall, Inc., New York, 1949, pp. 113-114.

8. Timoshenko, S.: loc. cit., pp. 319-320.

9. Southwell, R. V.: Proc. Roy. Soc., London, Series A, Vol. 135, p. 601, 1932.

10. Schliesser, M., and Lederman, S.: "Experiments on Thermal Buckling", WADC TR 57-69, Dec. 1956.

Lenna G. Smith
Aeronautical Engineering Dept.
Stanford University

thesH528
Thermal buckling of centrally heated cir
3 2768 002 05987 5
DUDLEY KNOX LIBRARY